The cGAS-STING pathway is dispensable in a mouse model of *LMNA*-cardiomyopathy despite nuclear envelope rupture

Atsuki En[1,2], Hanumakumar Bogireddi[1], Briana Thomas[1], Alexis Stutzman[3], Sachie Ikegami[3], Brigitte LaForest[3], Omar Almakki[3], Peter Pytel[4], Ivan P. Moskowitz[5], Kohta Ikegami[1,6]

[1]Division of Molecular Cardiovascular Biology, Cincinnati Children's Hospital Medical Center, Cincinnati, OH, USA

[2]Graduate School of Nanobioscience, Yokohama City University, Yokohama, Kanagawa, Japan

[3]Department of Pediatrics, The University of Chicago, Chicago, IL, USA

[4]Department of Pathology, The University of Chicago, Chicago, IL, USA

[5]Departments of Pediatrics, Pathology, and Human Genetics, The University of Chicago, Chicago, IL, USA

[6]Department of Pediatrics, University of Cincinnati College of Medicine, Cincinnati, OH, USA

Corresponding author: **Kohta Ikegami**, kohta.ikegami@cchmc.org

Format: **Letter**

ABSTRACT

Mutations in the nuclear Lamin A/C gene (*LMNA*) cause diverse degenerative disorders, including malignant dilated cardiomyopathy in adults. A prevailing hypothesis postulates that *LMNA* mutations cause nuclear envelope ruptures that trigger pathogenic inflammatory signaling via the cGAS-STING cytosolic DNA-sensing pathway. Here, we provide evidence against this hypothesis, using a mouse model of *LMNA*-related cardiomyopathy that mimics Lamin A/C protein reduction observed in patient cardiomyocytes. We observed that pervasive nuclear envelope ruptures preceded the onset of cardiac transcriptional modulation and dilated cardiomyopathy. Nuclear ruptures activated DNA damage response without causing immediate cardiomyocyte death. However, cGAS-STING downstream cytokine genes remained inactive in the mutant cardiomyocytes. Deleting *cGas* or *Sting* did not alleviate cardiomyopathy. Instead, extracellular matrix signaling was predicted to emanate from Lamin A/C-reduced cardiomyocytes to communicate with fibroblasts in the heart. These findings suggest that cGAS-STING is not a major pathogenetic contributor to *LMNA*-related dilated cardiomyopathy in adult humans.

INTRODUCTION

Lamin A/C, encoded by *LMNA*, are nuclear lamina proteins that provide structural integrity to the nuclear envelope in animal cells [1–4]. Mutations in *LMNA* cause a spectrum of degenerative disorders, collectively called laminopathies, including frequent dilated cardiomyopathy (*LMNA*-related DCM) [5–7]. *LMNA*-related DCM is prevalent in genetic DCM, accounting for 6–15% of all genetic DCM cases [8,9]. *LMNA*-related DCM is predominantly adult-onset and accompanied by highly penetrant conduction system disease, heart failure, and mortality [10–13]. The molecular pathogenesis of *LMNA*-related DCM and other laminopathies remains unknown. A common observation in *LMNA*-related DCM patients is a reduction of Lamin A/C proteins in the heart, most strongly in cardiomyocytes compared with other cardiac cells, regardless of whether the causative heterozygous mutation is missense, nonsense, or frame-shift [5,14–16]. Reduction of nuclear lamins weakens the nuclear envelope and can cause ruptures of the nuclear envelope [17–19]. Nuclear envelope ruptures have been observed in patients [5,14,20–22], animal models [19,23–28], and cell culture models [19,29] of *LMNA*-related DCM and laminopathies. However, contribution of nuclear envelope rupture to the pathogenesis of *LMNA*-related DCM remains undefined.

A prevailing hypothesis for *LMNA*-related DCM pathogenesis implicates the cGAS-STING pathway as a link between nuclear envelope rupture, inflammatory signaling, and DCM pathogenesis [25,26,30–32]. cGAS-STING is a cytosolic DNA-sensing innate immune mechanism, in which exposure of DNA to the cytoplasm causes cGAS binding to DNA and cell-autonomous STING-mediated cytokine transcription via activation of transcription factors IRF3 and NFkB [33,34]. cGAS-STING pathway activation has been observed in a cell culture model of progeria [35], in developing hearts deleted for *Lmna* [36], and in the heart following ischemic injury, pressure overload, or diabetic insult [37–40]. However, a direct link between nuclear envelope ruptures and the cGAS-STING activation in *LMNA*-related DCM has not been established. In this study, we test the prevailing hypothesis that the cGAS-STING pathway activation contributes to *LMNA*-related DCM using a mouse model and provide evidence against this hypothesis.

RESULTS

Lamin A/C reduction in cardiomyocytes causes dilated cardiomyopathy in adult mice

We established a mouse model of *LMNA*-related DCM using cardiomyocyte-specific deletion of the mouse *Lmna* gene. We combined the *Lmna-LoxP* allele [41] with the tamoxifen-inducible cardiomyocyte-specific *Cre* recombinase allele [42], to induce *Lmna* gene deletion in cardiomyocytes of adult mice aged 6-8 weeks (*Lmna*$^{F/F}$*-Myh6-MerCreMer*; *Lmna*^{CKO}) (**Fig. 1A**). Cardiomyocytes isolated from *Lmna*^{CKO} mice exhibited a reduction of Lamin A/C proteins to about half (Lamin A, 47%; Lamin C, 43%) of the wild-type level at 2 weeks post tamoxifen, despite nearly complete *Lmna*$^{F/F}$ allele recombination (**Fig. 1B; Fig. S1A, B**). Consistently, Lamin A/C proteins remained detectable in individual cardiomyocytes within *Lmna*^{CKO} hearts at 1, 2, and 3.5 weeks post tamoxifen by immunohistochemistry (**Fig. 1C**). The modest reduction of Lamin A/C protein following gene knockout was consistent with the reported long 4-week half-life of Lamin A/C in mouse hearts [43] and was also noted in a study using similar cardiomyocyte-specific *Lmna* knockout mice using a different *Lmna-LoxP* allele [23]. Thus, our mouse model reproduced the reduction but not elimination of Lamin A/C proteins observed in cardiomyocytes of adult *LMNA*-related DCM patients [5,16], allowing us to investigate the pathogenesis of this disease.

Adult *Lmna*^{CKO} mice developed progressive dilated cardiomyopathy despite incomplete Lamin A/C protein reduction, as reported previously [23]. Hearts of the *Lmna*^{CKO} mice were indistinguishable from wild-type hearts in gross morphology and contractile activity, as assessed by echocardiography, until 2 weeks post tamoxifen (**Fig. 1D; Fig. S1C**). However, at 3 weeks post tamoxifen, left ventricular ejection fraction significantly diminished (**Fig. 1E**). At 3.5 weeks post tamoxifen, *Lmna*^{CKO} hearts became severely dilated (**Fig. 1D**), with a significant reduction of ventricular wall thickness (**Fig. S1C**) and loss of systolic activity (**Fig. 1E**). *Lmna*^{CKO} mice consistently died between 3.5 weeks and 4.5 weeks post tamoxifen (**Fig. 1F**). Thus, the modest reduction of Lamin A/C proteins in cardiomyocytes was sufficient to cause dilated cardiomyopathy that progressed to heart failure, recapitulating a crucial aspect of human *LMNA*-related DCM.

We sought to identify the onset of molecular changes preceding the functional decline of *Lmna*^{CKO} hearts. To this end, we profiled the transcriptome of the heart at Days 7, 11, and 14 post tamoxifen, by RNA-seq. At Days 7 and 11 post tamoxifen, the transcriptome of *Lmna*^{CKO} hearts was almost identical to that of wild-type hearts (**Fig. 1G**). However, at Day 14 post tamoxifen, we observed strong transcriptional changes, with extensive transcriptional upregulation (1,751 genes) and modest transcriptional downregulation (351 genes) in *Lmna*^{CKO} hearts relative to the wild-type hearts (**Fig. 1G; Table S1**). The upregulated genes were highly overrepresented for genes implicated in inflammatory responses and innate immune pathways (**Fig. 1H**) and included the cGAG-STING-related genes such as *Cgas*, *Sting1*, *Ifit1*, and *Irf7* (**Fig. 1I**). The downregulated genes were overrepresented for gene

pathways for cardiomyocyte metabolism and function (**Fig. 1H**), consistent with the reduction of the contractile activity at later time points.

We examined whether upregulation of inflammation- and immune-related gene expression reflected an inflammatory response in the *Lmna*^{CKO} heart. We observed that *Lmna*^{CKO} hearts at 2 weeks post tamoxifen were populated with an increased number of CD45-positive leukocytes, many of which were positive for the macrophage marker CD68 (**Fig. 1J; Fig. S1D**), suggesting upregulated innate immune activity. We also observed increased interstitial collagen deposition in *Lmna*^{CKO} hearts at 2 weeks post tamoxifen that developed to extensive fibrosis by 3.5 weeks post tamoxifen (**Fig. 1K**). Thus, Lamin A/C reduction in adult cardiomyocytes resulted in extensive gains of inflammation- and innate immunity-related transcription, macrophage expansion, and initial fibrotic response at 2 weeks post tamoxifen, preceding the morphological and functional changes reflective of clinical DCM (**Fig. 1L**).

Lamin A/C reduction resulted in localized nuclear envelope rupture in cardiomyocytes

We examined the hypothesis that Lamin A/C reduction caused nuclear envelope rupture, triggering inflammatory response driven by cytoplasmic DNA-induced innate immunity [44,45]. Although nuclear envelope rupture has been noted in patients or other mouse models of *LMNA*-related DCM and laminopathies [5,14,20–23,27], the extent of this event in the heart and its relationship with the pathogenesis of cardiomyopathy remain undefined. We therefore investigated the nuclear structure in the heart tissue sections at 2 weeks post tamoxifen, immunostained for Lamin A/C. We observed protrusion of nuclear DNA from the nuclear envelope in cardiomyocytes of *Lmna*^{CKO} hearts, while this event was absent in wild-type hearts (**Fig. 2A**). Nuclei with protruded DNA were positive for Lamin A/C staining, indicating that partial reduction of Lamin A/C was sufficient to cause DNA protrusion. We further examined the heart sections at 2 weeks post tamoxifen by electron microscopy. We observed highly condensed chromatin protruding from the tip of the nucleus in cardiomyocytes (**Fig. 2B; Fig. S2A**). Moreover, the nuclear membrane was absent specifically at the location of DNA protrusion, suggesting that ruptures of the nuclear envelope allowed DNA to protrude from the nucleus.

To validate that the nuclear envelope had ruptured, we isolated cardiomyocytes from the heart at 2 weeks post tamoxifen and examined the distribution of nuclear envelope proteins by immunofluorescence. Lamin A/C signals were specifically lost at the tips of *Lmna*^{CKO} nuclei from which DNA protruded (**Fig. 2C; Fig. S2B**). The Lamin A/C-depleted nuclear tips also lost the perinuclear matrix protein PCM1, localized on the cytoplasmic side of the outer nuclear membrane [46], confirming that the nuclear envelope had locally ruptured (**Fig. 2C**). We quantified the frequency of nuclear envelope rupture, as defined by DNA protrusion through PCM1-depleted tips of the nucleus, in multinucleated cardiomyocytes, which constitute ~90% of cardiomyocytes in adult mouse hearts (**Fig. S2C, D**) [47]. At Day 11 post tamoxifen, 31% of *Lmna*^{CKO} multinucleated cardiomyocytes had one (14%)

129 or multiple (17%) ruptured nuclei (**Fig. 2D, E**). The rupture frequency increased to 54% (25% one
130 rupture; 29% multiple ruptures) at Day 14 post tamoxifen. We noted that ruptures were exclusively
131 localized at the tips of the nuclei elongated along the longitudinal axis of the cardiomyocytes (**Fig.**
132 **2A–C; Fig. S2A–D**). The frequent nuclear envelope ruptures at Day 11 post tamoxifen indicated that
133 nuclear envelope rupture preceded the earliest transcriptional changes observed in the mutant hearts
134 at Day 14 post tamoxifen.

135 Nuclear envelope rupture should cause unrestrained nucleocytoplasmic exchange. We tested
136 this prediction by introducing nuclear localization signal (NLS)-fused tdTomato protein specifically in
137 cardiomyocytes *in vivo*. NLS-tdTomato was exclusively localized to nuclei in wild-type cardiomyocytes
138 as well as unruptured nuclei in *Lmna*^{CKO} cardiomyocytes, as expected (**Fig. 2F; Fig. S2E**). However,
139 NLS-tdTomato signals significantly diminished in ruptured nuclei (**Fig. 2G**). Reciprocally, NLS-tdTomato
140 signals increased in the cytoplasm of *Lmna*^{CKO} cardiomyocytes bearing ruptured nuclei, but not in the
141 cytoplasm of wild-type cardiomyocytes or in the cytoplasm of *Lmna*^{CKO} cardiomyocytes without ruptured
142 nuclei. These data indicated that the nucleocytoplasmic barrier had been breached due to nuclear
143 envelope rupture in the cardiomyocytes of *Lmna*^{CKO} mice.

144 Nuclear envelope ruptures are often accompanied by activation of the DNA damage response
145 pathway, presumably due to the access of cytoplasmic DNases into the nucleus [27,48–52]. Consistent with
146 this notion, we observed an elevated number of cardiomyocyte nuclei positive for gamma-H2AX, a
147 modified histone implicated in DNA damage response, in *Lmna*^{CKO} hearts at 2 weeks and 3.5 weeks
148 post tamoxifen (**Fig. 2H**). However, we did not detect a statistically significant increase in cell death in
149 the myocardium at 2 weeks post tamoxifen, as assessed by the TUNEL assay (**Fig. 2I, J**). These data
150 suggested that frequent nuclear envelope rupture activated DNA damage response but did not cause
151 immediate cell death in adult cardiomyocytes.

152 Taken together, Lamin A/C reduction in cardiomyocytes resulted in nuclear envelope ruptures at
153 a high frequency, followed by the activation of inflammation-related transcription, followed by the
154 development of dilated cardiomyopathy in *Lmna*^{CKO} hearts (**Fig. 2K**).

155

156 **Absence of cGAS-STING-related transcriptional activation in *Lmna*^{CKO} cardiomyocytes**

157 We tested the prevailing hypothesis that nuclear envelope rupture activates the cGAS-STING cytosolic
158 DNA sensing pathway of innate immunity [44,45]. According to this hypothesis, cGAS-STING-dependent
159 cytokine transcription should occur within *Lmna*^{CKO} cardiomyocytes because the cGAS-STING pathway
160 operates autonomously within cells bearing cytoplasmic DNA [33,34]. We first investigated the protein
161 abundance of cGAS, the cytosolic DNA sensor, and STING, the essential mediator for the pathway, by
162 immunoblotting. Both cGAS and STING were present in control adult hearts, but their abundance within
163 wild-type and *Lmna*^{CKO} cardiomyocytes was very low (**Fig. S3A–D**).

We next defined the cell type-resolved transcriptional changes in *Lmna*^{CKO} hearts by single-nucleus RNA-seq (snRNA-seq) of wild-type and *Lmna*^{CKO} hearts. We obtained high-quality transcriptomes for a total of 14,111 nuclei originating from either wild-type hearts or *Lmna*^{CKO} hearts at 2 weeks post tamoxifen in biological triplicate (**Fig. 3A**). Using marker expression, we categorized the 14,111 nuclei into major cardiac cell types, namely cardiomyocytes (CM1 and CM2), fibroblasts (Fib1 and Fib2), macrophages (Mac1 and Mac2), T cells, endothelial cells, coronary endothelial cells, lymphatic endothelial cells, pericytes, and neurons (**Fig. S4A**). Among these, CM2, Fib2, Mac2, and T-cell populations were highly overrepresented by cells in *Lmna*^{CKO} hearts, whereas Fib1 was underrepresented in *Lmna*^{CKO} hearts (**Fig. 3B; Fig. S4B**). CM2 was characterized by high *Rtn4* expression, Fib2 by high myofibroblast marker *Postn* expression [53], and Mac2 by high circulating monocytic marker *Ccr2* expression [54] (**Fig. S4A**). Other cell populations did not exhibit biased representations in *Lmna*^{CKO} hearts compared to wild-type hearts. These analyses suggested that Lamin A/C reduction within cardiomyocytes strongly affected gene expression in cardiomyocytes, fibroblasts, and immune cells.

We asked whether cGAS-STING-related genes were upregulated within *Lmna*^{CKO} cardiomyocytes. We first identified the total set of differentially expressed genes within each cell type of *Lmna*^{CKO} hearts relative to wild-type hearts. We performed differential gene expression analysis on cardiomyocytes (consisting of CM1 and CM2), fibroblasts (consisting of Fib1 and Fib2), immune cells (consisting of Mac1, Mac2, and T cells), and the remaining individual cell populations. We observed extensive differential gene expression within cardiomyocytes (154 up- and 92 down-regulated), fibroblasts (448 up- and 272 down-regulated), and immune cells (253 up- and 251 down-regulated), while other cell types did not exhibit substantial expression differences (**Fig. 3C; Table S2**).

None of the canonical cGAS-STING-downstream genes, such as *Ifnb1*, *Cxcl10*, *Ifit1*, *Ifit3*, and *Irf7*, were upregulated within *Lmna*^{CKO} cardiomyocytes (**Fig. 3D; Fig. S4C**). Moreover, *Cgas* and *Sting1* transcripts were almost undetectable in both wild-type and *Lmna*^{CKO} cardiomyocytes, consistent with their low protein abundance. Unlike cGAS-STING-related genes, DNA damage response-related genes *Cdkn1a* and *Mdm2* were upregulated in *Lmna*^{CKO} cardiomyocytes (**Fig. 3E**), consistent with increased gamma-H2AX staining observed. Notably, cell death-related genes were not upregulated in *Lmna*^{CKO} cardiomyocytes (**Fig. S4D**), corroborating the negative TUNEL results. Furthermore, gene pathways related to the cytosolic-DNA-sensing and cytosolic pattern recognition were not overrepresented among the upregulated genes in *Lmna*^{CKO} cardiomyocytes (**Fig. 3F, G; Fig. S4E**). These results suggested that Lamin A/C reduction did not activate the cGAS-STING-dependent transcription in cardiomyocytes at 2 weeks post tamoxifen, despite frequent nuclear envelope ruptures.

Interestingly, we observed upregulation of cGAS-STING-related genes, including *Cxcl10*, *Ifit1*, and *Irf7*, in fibroblasts and immune cells of *Lmna*^{CKO} hearts (**Fig. 3D; Fig. S4C**). In contrast to

199 cardiomyocytes, both *Cgas* and *Sting* transcripts were abundantly expressed in wild-type cells.
200 Upregulated genes in fibroblasts and immune cells were also overrepresented for the cytosolic DNA
201 sensing pathway and other pattern recognition pathways (**Fig. 3G**). These observations suggested that
202 the reduction of Lamin A/C in cardiomyocytes indirectly activated cGAS-STING-related gene
203 expression in fibroblasts and immune cells.

204 To independently assess the absence of cGAS-STING-related expression within *Lmna*^{CKO}
205 cardiomyocytes, we employed SLAM-IT-seq to profile the transcriptome of both cardiomyocytes and
206 non-cardiomyocytes in the wild-type and *Lmna*^{CKO} hearts at 2 weeks post tamoxifen. SLAM-IT-seq
207 employs 4-thiouracil (4sU) to label transcripts in *Cre*-expressing cells *in vivo* (in our case,
208 cardiomyocytes), converts 4sU to C after total RNA isolation, and quantifies labeled and unlabeled
209 transcripts using high-throughput sequencing without requiring cell or nuclear isolations (**Fig. S5A;**
210 **Table S3**) [55]. As expected, cardiomyocyte-specific genes were specifically 4sU-labeled in wild-type
211 hearts (**Fig. S5B**). We then examined 4sU-labeling status of the 1,020 genes that were upregulated in
212 *Lmna*^{CKO} hearts by bulk RNA-seq at 2 weeks post tamoxifen (**Fig. 1G**) and measurable by
213 SLAM-IT-seq. Among these upregulated genes, 135 genes were 4sU-labeled, while 885 genes were
214 not 4sU-labeled in *Lmna*^{CKO} cardiomyocytes (**Fig. S5C**). None of the 4sU-labeled upregulated genes
215 included cytokine-related transcripts (**Fig. S5C**). Instead, immune-related genes were significantly
216 enriched among the unlabeled genes that were upregulated in *Lmna*^{CKO} hearts (**Fig. S5D**). These
217 observations suggested that immune/cytokine genes were upregulated in non-cardiomyocyte
218 populations, such as immune cells or fibroblasts, but not cardiomyocytes, within *Lmna*^{CKO} hearts. Thus,
219 two independent approaches suggested absence of cGAS-STING-related gene activation within
220 *Lmna*^{CKO} cardiomyocytes, despite the observed prevalent nuclear envelope rupture.

221

222 **Predicted ECM-mediated signaling from *Lmna*^{CKO} cardiomyocytes to fibroblasts**

223 The absence of overt cytokine transcription in *Lmna*^{CKO} cardiomyocytes suggested that
224 cytokine-independent signaling from *Lmna*^{CKO} cardiomyocytes may activate fibroblasts and immune
225 cells in the mutant hearts. We identified candidate intercellular communication type in *Lmna*^{CKO} hearts,
226 applying the CellChat program [56] on the snRNA-seq data at 2 weeks post tamoxifen. This analysis
227 nominated extracellular matrix (ECM)-receptor signaling from CM2 to Fib2 as the most strongly
228 upregulated communication originating from cardiomyocyte populations (**Fig. 3H**). Consistently,
229 collagen, integrin, and other ECM-related genes were upregulated in both cardiomyocytes and
230 fibroblasts in *Lmna*^{CKO} hearts (**Fig. S4F**), and ECM-related GO terms were among the most highly
231 upregulated pathways in cardiomyocytes and fibroblasts in *Lmna*^{CKO} hearts (**Fig. 3F**). ECM-related GO
232 term "proteoglycan in cancer" was also most highly enriched among 4sU-labeled upregulated genes in
233 SLAM-IT-seq (**Fig. S5D**). Interestingly, we did not identify direct upregulated communications between

234 cardiomyocytes and immune cell populations in *Lmna*^{CKO} hearts. Instead, Fib2 was predicted to act as a
235 central signaling hub, communicating with CM1, CM2, Fib2, and T cells via ECM-receptor signaling,
236 and with Mac2 via secreted signaling (**Fig. 3H**). Thus, ECM-mediated signaling, not cytokine-mediated
237 signaling, may initiate a proinflammatory intercellular communication cascade emanating from *Lmna*^{CKO}
238 cardiomyocytes. These analyses further underscored that nuclear envelope ruptures in *Lmna*^{CKO}
239 cardiomyocytes did not activate cGAS-STING-dependent cytokine signaling within cardiomyocytes
240 (**Fig. 3I**).
241

242 ***Cgas* or *Sting* deletion does not rescue dilated cardiomyopathy in *Lmna*^{CKO} mice**

243 Given the upregulation of certain cGAS-STING-related genes in fibroblasts and immune cells in
244 *Lmna*^{CKO} hearts (**Fig. 3D**), we investigated the potential involvement of the cGAS-STING pathway in
245 dilated cardiomyopathy in *Lmna*^{CKO} mice. Using the germline *Cgas* null and *Sting* null alleles[57,58], we
246 generated an experimental group, *Sting*$^{-/-}$;*Lmna*$^{F/F;Myh6MCM}$ (*Sting*$^{-/-}$;*Lmna*^{CKO}) mice, and corresponding
247 littermate control groups, *Sting*$^{+/+}$;*Lmna*$^{F/F;Myh6MCM}$ (*Sting*$^{+/+}$;*Lmna*^{CKO}), *Sting*$^{+/+}$;*Lmna*$^{F/+;Myh6MCM}$
248 (*Sting*$^{+/+}$;*Lmna*^{CHET}), and *Sting*$^{-/-}$;*Lmna*$^{F/+;Myh6MCM}$ (*Sting*$^{-/-}$;*Lmna*^{CHET}) mice. Similarly, we generated
249 *Cgas*$^{-/-}$;*Lmna*^{CKO} mice for the experimental group, along with littermate control groups *Cgas*$^{+/+}$;*Lmna*^{CKO},
250 *Cgas*$^{+/+}$;*Lmna*^{CHET}, and *Cgas*$^{-/-}$;*Lmna*^{CHET} mice. *Lmna* heterozygosity in adult cardiomyocytes
251 *(Lmna*^{CHET}*)*, employed as a control, exhibited no cardiac phenotype or lethality, consistent with a
252 previous report [41] (details below). We confirmed the complete absence of cGAS or STING proteins in
253 the *Cgas*$^{-/-}$ and *Sting*$^{-/-}$ hearts, respectively, by immunoblotting (**Fig. S3A–D**). By 3.5 to 4 weeks post
254 tamoxifen, the left ventricular ejection fraction in *Sting*$^{-/-}$;*Lmna*^{CKO} mice severely decreased to an extent
255 comparable to *Sting*$^{+/+}$;*Lmna*^{CKO} mice, whereas control *Sting*$^{+/+}$;*Lmna*^{CHET} and *Sting*$^{-/-}$;*Lmna*^{CHET} mice
256 maintained a normal ejection fraction (**Fig. 4A**). Corresponding with the functional decline,
257 *Sting*$^{-/-}$;*Lmna*^{CKO} hearts developed severe fibrosis similar to *Sting*$^{+/+}$;*Lmna*^{CKO} hearts by 3.5 to 4 weeks
258 post tamoxifen (**Fig. 4B**). Likewise, *Cgas*$^{-/-}$;*Lmna*^{CKO} hearts developed severe fibrosis similar to
259 *Cgas*$^{+/+}$;*Lmna*^{CKO} hearts (**Fig. 4B**). Moreover, both *Sting*$^{-/-}$;*Lmna*^{CKO} mice and *Cgas*$^{-/-}$;*Lmna*^{CKO} mice died
260 as early as *Sting*$^{+/+}$;*Lmna*^{CKO} or *Cgas*$^{+/+}$;*Lmna*^{CKO} mice by 4.5 weeks post tamoxifen, whereas no lethality
261 was observed in control *Lmna*^{CHET} mice, irrespective of the *Sting* or *Cgas* genotype (**Fig. 4C, D**). These
262 data indicated that the cGAS-STING pathway is dispensable for the pathophysiologic features of dilated
263 cardiomyopathy in *Lmna*^{CKO} hearts.

264 Finally, we investigated whether cGAS had contributed to the observed immune-related
265 transcriptional upregulation in *Lmna*^{CKO} hearts, by transcriptome profiling of hearts from
266 *Cgas*$^{-/-}$;*Lmna*^{CKO} mice and their respective littermate control mice. The transcriptome of
267 *Cgas*$^{-/-}$;*Lmna*^{CKO} hearts closely mirrored that of the control *Cgas*$^{+/+}$;*Lmna*^{CKO} hearts. Similarly, the
268 transcriptome of *Cgas*$^{-/-}$;*Lmna*^{CHET} hearts was almost identical to that of *Cgas*$^{+/+}$;*Lmna*^{CHET} hearts (**Fig.**

269 **4E; Table S4**). These results indicated that the cGAS-STING pathway did not contribute to the
270 transcriptional alterations observed in *Lmna*^{CKO} hearts, despite the observed frequent nuclear envelope
271 rupture (**Fig. 4F**).

DISCUSSION

Our findings revealed that the cGAS-STING pathway is dispensable for the development of dilated cardiomyopathy (DCM) in a mouse model of adult *LMNA*-related DCM that mimics the reduction of Lamin A/C protein observed in patient cardiomyocytes [5,16] (**Fig. 4F**). Our results challenge the notion that the cGAS-STING pathway plays a significant role in *LMNA*-related DCM, thereby questioning the potential efficacy of pharmacologically inhibiting cGAS as a treatment strategy for this condition that has been discussed [36,59].

Our conclusion diverges from a recent report that *Cgas* deletion can delay the development of early postnatal cardiomyopathy in mice lacking *Lmna* during embryonic and postnatal cardiac development [36]. We speculate that the exceptionally low expression of cGAS and STING within adult mouse cardiomyocytes is a primary factor contributing to the absence of cGAS-STING activation observed in our study. In contrast, it is possible that basal cGAS-STING activity is higher in neonatal, cell-cycle-active cardiomyocytes, given the strong association of cGAS-STING activity with an active cell cycle state [60,61]. Several mechanisms have been proposed to counteract cGAS recognition of DNA, including DNA binding competition with histones and BANF1, as well as heterochromatinization [44,62,63]. Our observed compaction of protruded nuclear DNA might have also contributed to the lack of cGAS response in *Lmna*^{CKO} cardiomyocytes within our mouse model.

Many reports suggest an association between DNA damage response and cGAS-STING activation, although the mechanistic link between these two processes remains unclear [36,64–67]. Our data, indicating that *Lmna*^{CKO} cardiomyocytes activate DNA damage response without activating the cGAS-STING pathway, suggests that DNA damage response and cGAS-STING activation can be uncoupled in specific cell types or states, such as adult cardiomyocytes.

A limitation of our study is its focus on the impact of Lamin A/C reduction exclusively within cardiomyocytes on the cGAS-STING pathway and the development of DCM. *LMNA*-related DCM patients may experience Lamin A/C reduction in other cell types, although it may also be more moderate than cardiomyocytes, as reported [5,16]. Whether Lamin A/C reduction in other cell types contributes to DCM through cGAS-STING activation remains an open question.

Nuclear envelope ruptures have been observed in *LMNA*-related DCM patients and animal models, but the timing of ruptures relative to disease onset has remained unclear. We observed that frequent nuclear envelope ruptures precede heart functional decline and transcriptional changes in *Lmna*^{CKO} hearts (**Fig. 4F**). The observation that nuclear envelope ruptures exclusively occur at the tips of elongated nuclei that are aligned to the longitudinal axis of cardiomyocytes suggests a link between the rupture process and the unique physical properties of adult cardiomyocytes or their nuclei. The mechanisms underlying nuclear envelope ruptures and the casual relationship between these events and the development of DCM require further investigation.

Beyond its implication in *LMNA*-related DCM, our study sheds light on how adult cardiomyocytes may react to cytoplasmic DNA. Adult cardiomyocytes may encounter cytoplasmic DNA due to factors like infection by bacteria or viruses, mitochondria damages, or mutations affecting genes encoding other nuclear envelope proteins [27,40,68–70]. We speculate that the adult cardiomyocytes are unable to respond to cytoplasmic DNA resulting from these pathological events via the cGAS-STING pathway.

The relationship between Lamin A/C and ECM has been described in the context of ECM-to-nucleus mechanotransduction wherein ECM modulation influences phosphorylation [71], folding [72], and expression [72,73] of Lamin A/C. However, the reciprocal impact of Lamin A/C modulation on ECM, as presented in this paper, has remained unexplored. An interesting implication of our analysis is that ECM gene upregulation in Lamin A/C-reduced cardiomyocytes serves as a signaling mechanism to activate fibroblasts in the heart. Nevertheless, we acknowledge that increased ECM gene expression has been observed in cardiomyocytes under some stress conditions [74–76]. Regardless of its specificity to Lamin A/C-reduced cardiomyocytes, ECM signaling warrants further investigation into laminopathy pathogenesis.

ACKNOWLEDGEMENT

We thank James Brainer and Jessica Webster for the assistance of electron microscopy. We thank core facilities for animal care, confocal microscopy, genomics, and pathology at Cincinnati Children's and the University of Chicago for assistance. This work is supported by NIH grant R21/R33 AG054770 (K.I.), Cincinnati Children's Research Innovation and Pilot grant (K.I.), NIH grant R01 HL092153, R01 HL124836, and R01 HL126509 (I.P.M).

AUTHOR CONTRIBUTION

Conceptualization, K.I.; Methodology, A.E. and K.I.; Formal Analysis, A.E. and K.I., Z.W.; Investigation, A.E., H.B., B.T., A.S., S.I., B.L., O.A., P.P., K.I.; Resources, I.P.M.; Data Curation, A.E. and K.I; Writing – Original Draft, A.E. and K.I.; Writing – Review & Editing, A.E. and K.I.; Visualization, A.E. and K.I.; Supervision, K.I.; Project Administration, K.I.; Funding Acquisition, K.I.

COMPETING INTEREST

None.

METHODS

Mouse genetics and treatment

Lmna-LoxP mice [41] were provided by Dr. Yixian Zheng at Carnegie Institution. *Myh6-MerCreMer* (Myh6MCM) transgene mice [42] (JAX stock No: 005657), *Rosa26*$^{CAG\text{-}LSL\text{-}tdTomato}$ mice [77] (JAX stock No: 25106), *Cgas-null* mice [58] (JAX stock No: 026554), and *CAG-Lox-Stop-Lox-Uprt* transgene mice [78] (*Uprt*^{Tg}; JAX stock No: 021469) were obtained from the Jackson Laboratory. *Sting-null* mice were generated by breeding *Sting-flox* mice [57], obtained from the Jackson Laboratory (JAX stock No: 031670), with mice carrying the *Mef2C-AHF-Cre* transgene allele [79], provided by Dr. Brian L. Black at University of California San Francisco. For cardiomyocyte-specific *Lmna* knockout experiments, *Lmna*$^{F/F}$*;Myh6MCM*$^{Tg/0}$ (*Lmna*^{CKO}) and *Lmna*$^{+/+}$*;Myh6MCM*$^{Tg/0}$ (wild-type control) mice were used. For the analysis of nuclear tdTomato intensity, *Lmna*$^{F/F}$*;Myh6MCM*$^{Tg/0}$;*Rosa26*$^{CAG\text{-}LSL\text{-}tdTomato/+}$ and *Lmna*$^{+/+}$*;Myh6MCM*$^{Tg/0}$;*Rosa26*$^{CAG\text{-}LSL\text{-}tdTomato/+}$ mice were used. For SLAM-IT-seq experiments, *Lmna*$^{F/F}$*;Myh6MCM*$^{Tg/0}$*;Uprt*$^{Tg/0}$, *Lmna*$^{+/+}$*;Myh6MCM*$^{Tg/0}$*;Uprt*$^{Tg/0}$, *Lmna*$^{F/F}$*;Myh6MCM*$^{Tg/0}$*;Uprt*$^{0/0}$, and *Lmna*$^{+/+}$*;Myh6MCM*$^{Tg/0}$*;Uprt*$^{0/0}$ mice were used. For *Cgas* deletion experiments, *Cgas*$^{-/-}$;*Lmna*$^{F/F}$*;Myh6MCM*$^{Tg/0}$ mice, *Cgas*$^{+/+}$;*Lmna*$^{F/F}$*;Myh6MCM*$^{Tg/0}$, *Cgas*$^{+/+}$;*Lmna*$^{F/+}$*;Myh6MCM*$^{Tg/0}$, and *Cgas*$^{-/-}$; *Lmna*$^{F/+}$*;Myh6MCM*$^{Tg/0}$ mice were used. For *Sting* deletion experiments, *Sting*$^{-/-}$;*Lmna*$^{F/F}$*;Myh6MCM*$^{Tg/Tg}$ mice, *Sting*$^{+/+}$;*Lmna*$^{F/F}$*;Myh6MCM*$^{Tg/Tg}$, *Sting*$^{+/+}$;*Lmna*$^{F/+}$*;Myh6MCM*$^{Tg/Tg}$, and *Sting*$^{-/-}$; *Lmna*$^{F/+}$*;Myh6MCM*$^{Tg/Tg}$ mice were used. All mice used in experiments were administered with tamoxifen (Sigma, T5648) at 6-8 weeks of age via intraperitoneal injections (100 μL of 4 mg/mL solution per day for 4 consecutive days) dissolved in corn oil (Sigma, C8267). All mice were used in mixed genetic backgrounds. All mouse experiments were approved by the Institutional Animal Care and Use Committee (IACUC) at Cincinnati Children's Hospital under IACUC protocol 2021-0014 or at University of Chicago under IACUC protocol 71730-10. All procedures were performed in compliance with institutional and governmental regulations under PHS Animal Welfare Assurance number D16-00068 (Cincinnati Children's) or D16-00322 (University of Chicago).

Echocardiography

The transthoracic echocardiography was performed using a Vevo 3100 LT (FUJI FILM VisualSonics) and a transducer of 50-MHz MX-700. The level of the papillary muscles, two-dimensional B-mode tracings were recorded in both long and short-axis views, followed by one-dimensional M-mode tracings in the both axes, with at least three consecutive cardiac cycles analyzed. Data was analyzed by using Vevo LAB Software Package V3.2.6. Echocardiographic parameters between two groups were compared using Wilcoxon rank sum tests, and P-values were adjusted for multiple testing using the Benjamini-Hochberg procedure in R.

372 **Survival analysis**

373 Kaplan-Meier survival analyses were performed using the *survival* package and visualized using the
374 *survminer* package in R. Log-rank tests were performed using the *survdiff* function in the survival
375 package.

376

377 **Histological staining**

378 Hearts were perfused with 100 mM KCl and fixed in 10% Formalin (Fisherbrand, 245-685). Fixed hearts
379 were embedded in paraffin and sectioned to a thickness of 5 μm. Heart sections were stained with
380 hematoxylin and eosin (H&E) or a Masson's Trichrome Kit (Thomas Scientific LLC, KTMTRPT)
381 according to the manufacturer's protocol.

382

383 **Cardiomyocyte isolation**

384 Mice were administered with heparin (100 Units, NDC 25021-400-10), anesthetized with Isoflurane, and
385 euthanized by cervical dislocation. Hearts were perfused with 100 mM KCl and moved to Tyrode's
386 solution (10 mM glucose, 5 mM HEPES, 5.4 mM KCl, 1.2 mM $MgCl_2$, 150 mM NaCl and 2 mM sodium
387 pyruvate, pH 7.35). Excised hearts were cannulated to the Langendorff retrograde perfusion system
388 through the aorta and perfused with Base solution (Tyrode's solution with 10 mM taurine and 12 mM
389 2,3-butanedione monoxime) and then digested with prewarmed Digestion buffer (Base solution with
390 180 U/mL Collagenase Type II (Worthington, LS004177) and 25 μM $CaCl_2$) for 20 minutes at 37°C.
391 Heart tissue was then isolated, gently minced in Base solution containing 5 mg/mL BSA. Cell
392 suspension was filtrated through a 240 μm mesh. Cardiomyocytes settled to the bottom of conical tubes
393 by gravity were used in experiments.

394

395 **Immunohistochemistry**

396 Deparaffinized heart tissue sections, that had been fixed with 10% formalin, were subjected to
397 heat-induced antigen retrieval in Target Retrieval Solution (S2367, DAKO) for 5 minutes.
398 Antigen-retrieved sections were incubated with anti-Lamin A/C antibody Ab26300 (rabbit, Abcam)
399 (1:400) for 1 hour at room temperature, followed by biotinylated anti-rabbit IgG antibody for 30 minutes
400 at room temperature. The antigen-antibody binding was detected by Elite kit (PK-6100, Vector
401 Laboratories) and DAB (DAKO, K3468) system. Sections were counterstained by hematoxylin.

402

403 **Immunofluorescence on tissue sections**

404 Deparaffinized heart tissue sections, that had been fixed with 10% formalin, were subjected to
405 heat-induced antigen retrieval in 10 mM Tris EDTA buffer (pH 9.0) for 5 minutes. Antigen-retrieved
406 sections were incubated overnight at 4 °C with goat anti-CD45 antibody (R&D Systems, AF114-SP) and

407 rabbit anti-CD68 antibody (Cell Signaling, 97778), or rabbit anti-γ-H2A.X antibody (Cell Signaling, 9718)
408 and goat anti-desmin antibody (Invitrogen, PA5-19063), followed by Alexa fluorophore-conjugated
409 secondary antibodies for 1 hour at 37 °C. Cells were counterstained with DAPI
410 (4′,6-diamidino-2-phenylindole), submerged in 0.25% Sudan Black B (Electron Microscopy Slides,
411 #21610) in 70% Isopropanol for 10 minutes, and then mounted with ProLong Glass Antifade Mountant
412 (Invitrogen, P36984). Fluorescence signals and imaging were acquired using a Nikon A1R
413 laser-scanning confocal microscope. CD45 and CD68 quantification of whole heart tissue was
414 performed using Nikon NIS-Elements; each genotype had five biological replicates. CD45/CD68
415 positive cells were identified based on the overlap of the DAPI signal with CD45/CD68. Signal
416 intensities between two groups were compared using Wilcoxon rank sum tests in R.
417

418 **Immunofluorescence on isolated cardiomyocytes**

419 Isolated cardiomyocytes were fixed in 4% paraformaldehyde (Electron Microscopy Slides, #15710) in
420 PHEM buffer (60 mM PIPES pH7.5, 25 mM HEPES pH7.5, 10 mM EGTA, 4 mM $MgSO_4$) for 10 minutes
421 at 37°C, then washed with PBS and attached to coverslips with Cell-Tak Cell Adhesive (Sigma Aldrich,
422 354240). Cells were blocked and permeabilized with in a buffer containing 5% normal donkey serum
423 (Jackson ImmunoResearch, 017-000-121), 1% non-fat milk, and 0.1% Triton X-100 in PBS for 1 hour at
424 37°C. Permeabilized cells were incubated overnight at 4°C with mouse anti-Lamin A/C antibody (Santa
425 Cruz, sc-376248) or rabbit anti-PCM-1 antibody (Sigma, HPA023370). Cells were washed and
426 incubated with Alexa fluorophore-conjugated secondary antibodies and Alexa Fluor Plus 647 Phalloidin
427 for 1 hour at 37°C. Cells were counterstained with DAPI and then mounted with ProLong Glass Antifade
428 Mountant. Fluorescence signals were detected on Nikon A1R laser-scanning confocal microscope or
429 Yokogawa CSU-W1 Sora spinning disk confocal microscope.
430

431 **Quantification of nuclear envelope ruptures**

432 Immunofluorescent images of isolated cardiomyocytes immuno-stained for PCM1 and counter-stained
433 with DAPI (DNA) and Phalloidin (F-actin) were used for nuclear envelope rupture quantification.
434 Rod-shape cardiomyocytes with a well-defined sarcomere structure based on Phalloidin staining that
435 had two or more nuclei were used for quantification. A nuclear envelope rupture event was defined as
436 an instance of DAPI signal protrusion from a location of the nuclear envelope at which PCM1 signals
437 were specifically discontinued. The percentage of cells with one or more ruptured nuclei and the
438 number of ruptured nuclei per cell were quantified manually using the Nikon NIS-Elements image
439 analysis software.

440 For quantification of NLS-tdTomato intensities, *Lmna*$^{F/F}$;*Myh6MCM*$^{Tg/0}$;*Rosa26*$^{CAG\text{-}LSL\text{-}tdTomato/+}$ and
441 *Lmna*$^{+/+}$;*Myh6MCM*$^{Tg/0}$;*Rosa26*$^{CAG\text{-}LSL\text{-}tdTomato/+}$ mice were used. Isolated cardiomyocytes were fixed,

442 immunostained for PCM1, and counterstained with DAPI. Quantification of NLS-tdTomato signals was
443 performed in the Fiji image analysis software. Cardiomyocytes that had two or more nuclei were used
444 for quantification. Nuclei with nuclear envelope ruptures were identified as described above. A
445 freehand-drawn area was placed inside a nucleus for quantification of the nuclear tdTomato signal. A
446 single nucleus was selected for quantification using the following algorithm: If a cell had only ruptured
447 nuclei, one ruptured nucleus was randomly selected for quantification; then, if a cell had both ruptured
448 and unruptured nuclei, one ruptured nucleus was randomly selected for quantification; then, if a cell had
449 only unruptured nuclei, one unruptured nucleus was randomly selected for quantification. A second
450 quantification area of the same size as the nuclear area was placed in the cytoplasm for cytoplasmic
451 tdTomato signal quantification. For each of the two areas, a mean NLS-tdTomato pixel intensity was
452 measured using the ROI manager function in Fiji. Signal intensities between two groups were
453 compared using Wilcoxon rank sum tests, and P-values were adjusted for multiple testing using the
454 Benjamini-Hochberg procedure in R.
455
456 **TUNEL assay**
457 TUNEL assays were performed on deparaffinized heart sections using a Click-iT™ Plus TUNEL Assay
458 Kits for In Situ Apoptosis Detection (Invitrogen, C10617), according to the manufacturer's instruction.
459 The samples were then co-stained with Alexa Fluor Plus 647 Phalloidin (Invitrogen, A30107) for 1 hour
460 at 37°C to visualize cells in tissue sections. For positive controls, sample tissues were treated with
461 DNase I prior to the TUNEL assay. The number of cells with positive staining in the TUNEL assay
462 (TUNEL^{+} cells) was determined using sections from three hearts per genotype. TUNEL positive cell
463 counts between two groups were compared using Wilcoxon rank sum tests in R.
464
465 **Immunoblot**
466 Snap-frozen hearts or isolated cardiomyocytes were lysed in the RIPA buffer (20 mM Tris-HCl, 150 mM
467 NaCl, 1% IGEPAL, 0.5% sodium deoxycholate, 0.1% SDS, 10 mM dithiothreitol, protease and
468 phosphatase inhibitors) or the Urea buffer (20 mM HEPES pH 7.4, 1 M NaCl, 8 M urea, protease and
469 phosphatase inhibitors). Proteins were extracted using pestle homogenization and sonication. Cell
470 lysates were centrifuged at 13,000 rpm for 5 minutes at 4°C, and proteins in the supernatant were
471 separated by SDS-PAGE. Proteins were transferred to a PVDF membrane. Membranes were blocked
472 with nonfat milk. The primary antibodies were rabbit anti-Lamin A/C antibody (Santa Cruz, sc-20681,
473 1:1000), rabbit anti-cGAS antibody (Cell Signaling, #31659, 1:500), rabbit anti-STING antibody (Cell
474 Signaling, #13647, 1:500), and rabbit anti-GAPDH antibody (ABclonal, AC001, 1:1000); Secondary
475 antibodies: anti-rabbit/mouse IgG (H+L) DyLight 680 and 800 (Cell Signaling, 1:5000). Signals were

476 detected and quantified in the Odyssey CLx Imager (LI-COR). The gel after protein transfer was
477 counter-stained by Coomassie to evaluate the loaded protein amount.
478
479 **Electron microscopy**
480 Heart tissues were dissected and fixed in 2.5% glutaraldehyde, post-fixed in 1% OsO4 for 1 hour at
481 4°C, rinsed, dehydrated in ethanol, and infiltrated overnight. The semithin Epon sections were screened
482 by light microscopy to select areas with longitudinal orientation of myocytes that were subsequently
483 processed to prepare thin sections. Those were stained with 1% uranyl acetate, followed by lead
484 citrate.
485
486 **RNA-seq**
487 For RNA-seq comparing wild-type mice with *Lmna*^{CKO} mice at different post tamoxifen times, we used
488 wild-type (n=5) and *Lmna*^{CKO} mice (n=4) at 1 week post tamoxifen, wild-type (n=3) and *Lmna*^{CKO} mice
489 (n=2) at 11 days post tamoxifen, and wild-type (n=7) and *Lmna*^{CKO} mice (n=5) at 2 weeks post
490 tamoxifen. For RNA-seq analysis of *Lmna/Cgas* double knockout mice, we used *Cgas*$^{-/-}$;*Lmna*$^{F/F;Myh6MCM}$
491 mice (n=4), *Cgas*$^{+/+}$;*Lmna*$^{F/F;Myh6MCM}$ (n=6), *Cgas*$^{+/+}$;*Lmna*$^{F/+;Myh6MCM}$ (n=6), and *Cgas*$^{-/-}$;*Lmna*$^{F/+;Myh6MCM}$
492 (n=4) for experiments. Hearts were perfused with 100 mM KCl and removed for RNA extraction. Total
493 RNAs were extracted with Trizol LS (Invitrogen, 10296010), treated with DNaseI, and purified. For
494 tamoxifen time course experiments, mRNA sequencing libraries were generated using the poly-A
495 selection module in the NEBNext UltraII Directional RNA Library Prep Kit (NEB E7760) and sequenced
496 on the Illumina HiSeq 2500 sequencer with single-end 50 cycles. For cGas/Lmna double knockout
497 experiments, libraries were generated using QuantSeq 3' mRNA-Seq Library Prep Kit FWD (Lexogen,
498 K01596) and sequenced on the Illumina NovaSeq 6000 sequencer with single-end 100 cycles.
499
500 **RNA-seq analysis**
501 High-throughput sequencing reads were aligned to the mouse mm39 reference genome with the
502 Gencode vM27 basic annotation using STAR version 2.7.9 [80] with the default alignment parameters
503 except "clip3pAdapterSeq AGATCGGAAGAGCACACGTCTGAACTCCAGTCA". From raw read counts
504 per transcript, TPM (transcripts per million) was calculated in R as follows: TPM=10^6 x RPK/sum(RPK),
505 where RPK=read count/transcript length in kp, and sum(RPK) is the sum of RPKs for all transcripts.
506 Raw read counts were used for differential gene expression analyses using DESeq2 [81] in R.
507 Protein-coding or lncRNA genes with adjusted P-value < 0.05 and absolute $\log_2$ fold change > 1 were
508 considered differentially expressed genes (**Table S1 & Table S4**). Differentially expressed genes were
509 analyzed for the enrichment of GO Biological Processes, GO Molecular Functions, GO Cellular
510 Components, and KEGG pathway terms using Metascape [82] with the default enrichment parameters.

511

512 **Single-nucleus RNA-seq**

513 For single-nucleus RNA-seq, we used wild-type (n=3) and *Lmna*^{CKO} mice (n=3) at 2 weeks post
514 tamoxifen. Combinatorial indexing-based single-nucleus RNA-seq was conducted according to the
515 optimized sci-RNA-seq3 protocol developed previously [83]. Briefly, mice were anesthetized with
516 isoflurane, euthanized by cervical dislocation, and then hearts were perfused with 100 mM KCl.
517 Removed hearts were diced into small pieces in cold PBS containing Diethyl pyrocarbonate (DEPC,
518 Sigma D5758). Fresh heart pieces were dounce-homogenized to liberate nuclei in Hypotonic lysis
519 buffer B (7.7 mM Na_2HPO_4, 4.5 mM NaH_2PO_4, 1.8 mM KH_2PO_4, 2.7 mM KCl, 10.3 mM NaCl, 3 mM
520 $MgCl_2$, 0.08% BSA, 0.025% Igepal CA-630, 1% DEPC) and passed through cell strainers. Nuclei were
521 fixed in 1 mg/mL dithiobis(succinimidyl propionate) (DSP, Thermo Fisher 22585) for 15 min on ice,
522 washed, and stored at –80°C until use. For each mouse, 50,000 nuclei were placed in each of 8 wells
523 of a 96-well plate (total 48 wells for 6 mice). The remaining 48 wells were filled with similarly processed
524 mouse heart nuclei with comparable sample quality from an unrelated project. Nuclei were subjected to
525 reverse-transcription with 96-indexed poly-T RT primers that contained a unique molecular identifier
526 (UMI) sequence (3lvl_mRNA_RT_plate_1; **Table S5**). Nuclei from all wells were combined and
527 redistributed evenly to 96 wells. Redistributed cells were subjected to ligation with 96-indexed ligation
528 primers in 96 wells (3lvl_mRNA_Lig_plate_1; **Table S6**). Nuclei from all wells were combined again and
529 redistributed evenly to 96 wells at 1,000 nuclei per well. Redistributed cells underwent second strand
530 synthesis, protease digestion, tagmentation using N7-loaded Tn5 transposase, and PCR-amplified
531 using 96-indexed PCR P7 primers (PCR_P7_plate1; **Table S7**) and the unindexed P5 primer, for 16
532 cycles. PCR amplicons were combined and size-selected for DNA fragments between 250 bp and 600
533 bp. Purified library DNA were sequenced for 50 bases on the paired-end mode (34 cycles on Read1 to
534 sequence the ligation index, UMI, and the RT barcode; 10 cycles on Index1 to sequence the P7 index;
535 and 48 cycles on Read2 to sequence the cDNA) using an Illumina NovaSeq6000 sequencer.

536

537 **Single-nucleus RNA-seq analysis**

538 Pre-processing of the single-nucleus RNA-seq data was performed using the published sci-RNA-seq3
539 pipeline [83], available in Github (https://github.com/JunyueC/sci-RNA-seq3_pipeline). The sci-RNA-seq3
540 pipeline takes fastq files separated by the P7 index as input, aligns reads to the genome, and returns a
541 gene-by-cell read count matrix. First, raw reads were trimmed to remove poly A tails, aligned to the
542 mm39 mouse reference genome using STAR, and filtered for MAPQ greater than or equal to 30.
543 Duplicate reads were removed based on UMI. Read counts per gene were computed for each cell
544 defined by the unique combination of the RT index, ligation index, and P7 index. The gene-by-cell count
545 matrix produced by the sci-RNA-seq3 pipeline was further processed in the *SingleCellExperiment*

546 package framework in R [84]. We used the *scDblFinder* package for doublet detection and the *scuttle*
547 package for mitochondrial RNA quantification in R. We obtained 14,111 cells after filtering for cells with
548 the *scDblFinder* doublet score less than 0.25 and mitochondrial RNA contamination percentage less
549 than 2% of total RNAs per cell. Read counts for a gene were normalized by per-cell read depth and
550 then log-transformed to obtain normalized expression values ("logcounts"). Logcounts were used to plot
551 expression values in graphs. Principal component analysis (PCA) was performed on logcounts for
552 2,000 highly variable genes across cells using the *fixedPCA* function in the *scran* package. The top 50
553 principal components were used in the *runUMAP* function in the *scater* package with n_neighbors=20
554 and min_dist=1 parameters to obtain UMAP dimensions. To cluster cells, logcounts were processed in
555 the *clusterCells* function in the *scran* package using the top 50 principal components, with the number
556 of nearest neighbors k=12. Cell clusters were annotated manually with cell type names based on
557 marker gene expression. Per-gene read counts were summed within cell groups and processed by the
558 *DESeq2* package [81] to perform pseudo-bulk differential gene expression analysis. Genes with adjusted
559 P-values smaller than 0.05 were defined as differentially expressed genes (**Table S2**). GO analysis of
560 differentially expressed genes was performed as described in the RNA-seq analysis section. For the
561 analysis for the enrichment within selected GO and KEGG terms, all genes associated with the
562 selected terms were obtained using the R packages *GO.db* and *KEGGREST*, and enrichment of
563 differentially expressed genes among these genes was computed by Fisher's exact test with P-values
564 adjusted by the Benjamini-Hochberg procedure. Cell-cell communication analysis was performed using
565 the *CellChat* package in R [56] using the 12 cell type annotations and the default mouse database with a
566 minimum of ten cells for the analysis. Positive communications were selected by the
567 *subsetCommunication* function with threshold P-value less than 0.05, and the reported interaction
568 counts were used to plot data.
569

570 **SLAM-IT-seq**

571 For SLAM-IT-seq experiments, we used *Lmna*$^{F/F}$*;Myh6MCM*$^{Tg/0}$*;Uprt*$^{Tg/0}$ (n=6) and
572 *Lmna*$^{+/+}$*;Myh6MCM*$^{Tg/0}$*;Uprt*$^{Tg/0}$ (n=8) mice as experimental groups, and *Lmna*$^{F/F}$*;Myh6MCM*$^{Tg/0}$*;Uprt*$^{0/0}$
573 (n=4) and *Lmna*$^{+/+}$*;Myh6MCM*$^{Tg/0}$*;Uprt*$^{0/0}$ (n=3) mice as negative control groups that would not
574 incorporate 4-thiouracil (4sU) due to the absence of the *Uprt* allele. All mice were administered with
575 tamoxifen and used at 2 weeks post tamoxifen treatment. SLAM-IT-seq was conducted according to a
576 previously established protocol [53]. Briefly, mice were intraperitoneally injected with 4-thiouracil (4sU)
577 dissolved in a DMSO/corn oil (1:3) solution at a dose of 10 mg per gram of body weight. Six hours after
578 the injection, mice were sacrificed, and hearts were perfused with 100 mM KCl and removed. RNAs
579 from the left ventricular free wall were extracted by Trizol LS and purified and DNaseI treated using
580 Directzol RNA miniprep kit (Zymo, R2052). Purified RNAs (1.5 µg) were subjected to alkylation in the

presence of 12 mM Iodoacetamide (IAA, Sigma I1149). High-throughput sequencing libraries were generated from the alkylated RNAs using Quant-seq 3' mRNA-seq FWD kit (Lexogen K01596) and sequenced 100 bases on the single-end mode on an Illumina NovaSeq6000 sequencer.

SLAM-IT-seq analysis

We analyzed SLAM-IT-seq data according to the published SLAM-IT-seq data analysis pipeline that uses the *slamdunk* package [85], available in Github (https://github.com/t-neumann/slamdunk), and R functions [55]. First, raw reads were processed by the *slamdunk all* function in the the *slamdunk* package with the following alignment parameters: --trim-5p 12 --topn 100 --multimap --max-read-length 101 with default --var-fraction (0.8) and default -c (1). This function aligned reads to 3' UTRs of Gencode vM27 genes (total 208,307 UTRs from 37,065 unique genes) in the mm39 mouse reference genome. Aligned reads were processed by the *alleyoop utrrates* function in the *slamdunk* package with default parameters to quantify C-to-T conversion events. UTRs with at least one read coverage for all 21 samples were retained for further analyses (47,717 UTRs from 14,250 unique genes). Statistically significant C-to-T conversion events in each transcript (i.e. the likelihood of cardiomyocyte-derived transcripts) were identified by comparing the conversion events in mice carrying the *Uprt* allele with those in mice not carrying this allele using beta binomial test (*bbtest* function) in R. P-values of the beta binomial test were adjusted with the Benjamini-Hochberg procedure for multiple tests (**Table S3**). A transcript with the lowest adjusted P-value was chosen to represent a gene if there were multiple transcripts per gene. Genes with the adjusted P-values smaller than 0.05 were defined as originating from cardiomyocytes, whereas genes with adjusted P-values greater than or equal to 0.05 were defined as not originating from cardiomyocytes.

DATA AVAILABILITY

High-throughput sequencing data associated with this version of the manuscript are limited to reviewers and journal editors. All data will become available to the public after peer review.

SUPPLEMENTARY TABLES

Table S1. Differentially expressed genes between wild-type and *Lmna*^{CKO} hearts at 1 week, 11 days, or 2 weeks post tamoxifen, derived from RNA-seq.

Table S2. Differentially expressed genes between cells of wild-type and *Lmna*^{CKO} hearts, derived from pseudo-bulk analysis of snRNA-seq data.

615 **Table S3.** Normalized expression values, C-to-T conversion rates, and beta-binomial test P-values for
616 SLAM-IT-seq data.
617
618 **Table S4.** Differentially expressed genes for *Cgas/Lmna* double-knockout analysis, derived from
619 RNA-seq.
620
621 **Table S5.** Indexed RT primers for snRNA-seq.
622
623 **Table S6.** Indexed ligation primers for snRNA-seq.
624
625 **Table S7.** Indexed P7 PCR primers for snRNA-seq.

REFERENCES

1. Aebi, U., Cohn, J., Buhle, L. & Gerace, L. The nuclear lamina is a meshwork of intermediate-type filaments. *Nature* **323,** 560–564 (1986).
2. Goldman, A. E., Maul, G., Steinert, P. M., Yang, H. Y. & Goldman, R. D. Keratin-like proteins that coisolate with intermediate filaments of BHK-21 cells are nuclear lamins. *Proc. Natl. Acad. Sci. U. S. A.* **83,** 3839–3843 (1986).
3. Röber, R. A., Weber, K. & Osborn, M. Differential timing of nuclear lamin A/C expression in the various organs of the mouse embryo and the young animal: a developmental study. *Development* **105,** 365–378 (1989).
4. Dechat, T., Pfleghaar, K., Sengupta, K., Shimi, T., Shumaker, D. K., Solimando, L. & Goldman, R. D. Nuclear lamins: major factors in the structural organization and function of the nucleus and chromatin. *Genes Dev.* **22,** 832–853 (2008).
5. Arbustini, E., Pilotto, A., Repetto, A., Grasso, M., Negri, A., Diegoli, M., Campana, C., Scelsi, L., Baldini, E., Gavazzi, A. & Tavazzi, L. Autosomal dominant dilated cardiomyopathy with atrioventricular block: a lamin A/C defect-related disease. *J. Am. Coll. Cardiol.* **39,** 981–990 (2002).
6. van Tintelen, J. P., Hofstra, R. M. W., Katerberg, H., Rossenbacker, T., Wiesfeld, A. C. P., du Marchie Sarvaas, G. J., Wilde, A. A. M., van Langen, I. M., Nannenberg, E. A., van der Kooi, A. J., Kraak, M., van Gelder, I. C., van Veldhuisen, D. J., Vos, Y., van den Berg, M. P. & Working Group on Inherited Cardiac Disorders, line 27/50, Interuniversity Cardiology Institute of The Netherlands. High yield of LMNA mutations in patients with dilated cardiomyopathy and/or conduction disease referred to cardiogenetics outpatient clinics. *Am. Heart J.* **154,** 1130–1139 (2007).
7. Worman, H. J., Fong, L. G., Muchir, A. & Young, S. G. Laminopathies and the long strange trip from basic cell biology to therapy. *J. Clin. Invest.* **119,** 1825–1836 (2009).
8. Parks, S. B., Kushner, J. D., Nauman, D., Burgess, D., Ludwigsen, S., Peterson, A., Li, D., Jakobs, P., Litt, M., Porter, C. B., Rahko, P. S. & Hershberger, R. E. Lamin A/C mutation analysis in a cohort of 324 unrelated patients with idiopathic or familial dilated cardiomyopathy. *Am. Heart J.* **156,** 161–169 (2008).
9. Hershberger, R. E. & Morales, A. in *GeneReviews®* (eds. Adam, M. P., Ardinger, H. H., Pagon, R. A., Wallace, S. E., Bean, L. J. H., Stephens, K. & Amemiya, A.) (University of Washington, Seattle, 2008). at <https://www.ncbi.nlm.nih.gov/pubmed/20301717>
10. Taylor, M. R. G., Fain, P. R., Sinagra, G., Robinson, M. L., Robertson, A. D., Carniel, E., Di Lenarda, A., Bohlmeyer, T. J., Ferguson, D. A., Brodsky, G. L., Boucek, M. M., Lascor, J., Moss, A. C., Li, W.-L. P., Stetler, G. L., Muntoni, F., Bristow, M. R. & Mestroni, L. Natural history of dilated cardiomyopathy due to lamin A/C gene mutations. *J. Am. Coll. Cardiol.* **41,** 771–780 (2003).
11. Sébillon, P., Bouchier, C., Bidot, L. D., Bonne, G., Ahamed, K., Charron, P., Drouin-Garraud, V.,

661 Millaire, A., Desrumeaux, G., Benaïche, A., Charniot, J.-C., Schwartz, K., Villard, E. & Komajda, M.
662 Expanding the phenotype of LMNA mutations in dilated cardiomyopathy and functional
663 consequences of these mutations. *J. Med. Genet.* **40,** 560–567 (2003).
664 12. van Rijsingen, I. A. W., Nannenberg, E. A., Arbustini, E., Elliott, P. M., Mogensen, J., Hermans-van
665 Ast, J. F., van der Kooi, A. J., van Tintelen, J. P., van den Berg, M. P., Grasso, M., Serio, A.,
666 Jenkins, S., Rowland, C., Richard, P., Wilde, A. A. M., Perrot, A., Pankuweit, S., Zwinderman, A.
667 H., Charron, P., Christiaans, I. & Pinto, Y. M. Gender-specific differences in major cardiac events
668 and mortality in lamin A/C mutation carriers. *Eur. J. Heart Fail.* **15,** 376–384 (2013).
669 13. Charron, P., Arbustini, E. & Bonne, G. What Should the Cardiologist know about Lamin Disease?
670 *Arrhythm Electrophysiol Rev* **1,** 22–28 (2012).
671 14. Verga, L., Concardi, M., Pilotto, A., Bellini, O., Pasotti, M., Repetto, A., Tavazzi, L. & Arbustini, E.
672 Loss of lamin A/C expression revealed by immuno-electron microscopy in dilated cardiomyopathy
673 with atrioventricular block caused by LMNA gene defects. *Virchows Arch.* **443,** 664–671 (2003).
674 15. Kato, K., Ohno, S., Sonoda, K., Makiyama, T., Ozawa, T. & Horie, M. Splice site mutation of LMNA
675 causes severe dilated cardiomyopathy via strong dominant reduction of total lamin expression. *Eur.*
676 *Heart J.* **41,** (2020).
677 16. Narula, N., Favalli, V., Tarantino, P., Grasso, M., Pilotto, A., Bellazzi, R., Serio, A., Gambarin, F. I.,
678 Charron, P., Meder, B., Pinto, Y., Elliott, P. M., Mogensen, J., Bolognesi, M., Bollati, M. & Arbustini,
679 E. Quantitative expression of the mutated lamin A/C gene in patients with cardiolaminopathy. *J.*
680 *Am. Coll. Cardiol.* **60,** 1916–1920 (2012).
681 17. Davidson, P. M. & Lammerding, J. Broken nuclei--lamins, nuclear mechanics, and disease. *Trends*
682 *Cell Biol.* **24,** 247–256 (2014).
683 18. Chen, N. Y., Yang, Y., Weston, T. A., Belling, J. N., Heizer, P., Tu, Y., Kim, P., Edillo, L., Jonas, S. J.,
684 Weiss, P. S., Fong, L. G. & Young, S. G. An absence of lamin B1 in migrating neurons causes
685 nuclear membrane ruptures and cell death. *Proc. Natl. Acad. Sci. U. S. A.* **116,** 25870–25879
686 (2019).
687 19. Cho, S., Vashisth, M., Abbas, A., Majkut, S., Vogel, K., Xia, Y., Ivanovska, I. L., Irianto, J., Tewari,
688 M., Zhu, K., Tichy, E. D., Mourkioti, F., Tang, H.-Y., Greenberg, R. A., Prosser, B. L. & Discher, D.
689 E. Mechanosensing by the Lamina Protects against Nuclear Rupture, DNA Damage, and
690 Cell-Cycle Arrest. *Dev. Cell* **49,** 920–935.e5 (2019).
691 20. Sylvius, N., Bilinska, Z. T., Veinot, J. P., Fidzianska, A., Bolongo, P. M., Poon, S., McKeown, P.,
692 Davies, R. A., Chan, K.-L., Tang, A. S. L., Dyack, S., Grzybowski, J., Ruzyllo, W., McBride, H. &
693 Tesson, F. In vivo and in vitro examination of the functional significances of novel lamin gene
694 mutations in heart failure patients. *J. Med. Genet.* **42,** 639–647 (2005).
695 21. Siu, C.-W., Lee, Y.-K., Ho, J. C.-Y., Lai, W.-H., Chan, Y.-C., Ng, K.-M., Wong, L.-Y., Au, K.-W., Lau,

Y.-M., Zhang, J., Lay, K. W., Colman, A. & Tse, H.-F. Modeling of lamin A/C mutation premature cardiac aging using patient-specific induced pluripotent stem cells. *Aging* **4,** 803–822 (2012).

22. Fan, Y., Tan, D., Zhang, X., Song, D., Chang, X., Wang, S., Yan, H., Ge, L., Yang, H., Bönnemann, C., Liu, J., Wang, S., Wu, X., Zhang, H. & Xiong, H. Nuclear Factor-κB Pathway Mediates the Molecular Pathogenesis of LMNA-Related Muscular Dystrophies. *Biochem. Genet.* **58,** 966–980 (2020).
23. Chai, R. J., Werner, H., Li, P. Y., Lee, Y. L., Nyein, K. T., Solovei, I., Luu, T. D. A., Sharma, B., Navasankari, R., Maric, M., Sim, L. Y. E., Loh, Y. J., Aliwarga, E., Cheong, J. W. L., Chojnowski, A., Autio, M. I., Haiyang, Y., Boon Tan, K. K., Keng, C. T., Ng, S. L., Chew, W. L., Ferenczi, M., Burke, B., Foo, R. S. Y. & Stewart, C. L. Disrupting the LINC complex by AAV mediated gene transduction prevents progression of Lamin induced cardiomyopathy. *Nat. Commun.* **12,** 4722 (2021).
24. Earle, A. J., Kirby, T. J., Fedorchak, G. R., Isermann, P., Patel, J., Iruvanti, S., Moore, S. A., Bonne, G., Wallrath, L. L. & Lammerding, J. Mutant lamins cause nuclear envelope rupture and DNA damage in skeletal muscle cells. *Nat. Mater.* **19,** 464–473 (2020).
25. Chen, R., Buchmann, S., Kroth, A., Arias-Loza, A.-P., Kohlhaas, M., Wagner, N., Grüner, G., Nickel, A., Cirnu, A., Williams, T., Maack, C., Ergün, S., Frantz, S. & Gerull, B. Mechanistic Insights of the LEMD2 p.L13R Mutation and Its Role in Cardiomyopathy. *Circ. Res.* **132,** e43–e58 (2023).
26. Kim, P. H., Chen, N. Y., Heizer, P. J., Tu, Y., Weston, T. A., Fong, J. L.-C., Gill, N. K., Rowat, A. C., Young, S. G. & Fong, L. G. Nuclear membrane ruptures underlie the vascular pathology in a mouse model of Hutchinson-Gilford progeria syndrome. *JCI Insight* **6,** (2021).
27. Ross, J. A., Arcos-Villacis, N., Battey, E., Boogerd, C., Avalos Orellana, C., Marhuenda, E., Swiatlowska, P., Hodzic, D., Prin, F., Mohun, T., Catibog, N., Tapia, O., Gerace, L., Iskratsch, T., Shah, A. M. & Stroud, M. J. Lem2 is essential for cardiac development by maintaining nuclear integrity. *Cardiovasc. Res.* (2023). doi:10.1093/cvr/cvad061
28. Zhang, Y., Ramirez-Martinez, A., Chen, K., McAnally, J. R., Cai, C., Durbacz, M. Z., Chemello, F., Wang, Z., Xu, L., Bassel-Duby, R., Liu, N. & Olson, E. N. Net39 protects muscle nuclei from mechanical stress during the pathogenesis of Emery-Dreifuss muscular dystrophy. *J. Clin. Invest.* **133,** (2023).
29. De Vos, W. H., Houben, F., Kamps, M., Malhas, A., Verheyen, F., Cox, J., Manders, E. M. M., Verstraeten, V. L. R. M., van Steensel, M. A. M., Marcelis, C. L. M., van den Wijngaard, A., Vaux, D. J., Ramaekers, F. C. S. & Broers, J. L. V. Repetitive disruptions of the nuclear envelope invoke temporary loss of cellular compartmentalization in laminopathies. *Hum. Mol. Genet.* **20,** 4175–4186 (2011).
30. Eissenberg, J. C. & Gonzalo, S. Pushing the limit on laminopathies. *Nat. Mater.* **19,** 378–380 (2020).

731 31. Gauthier, B. R. & Comaills, V. Nuclear Envelope Integrity in Health and Disease: Consequences on
732 Genome Instability and Inflammation. *Int. J. Mol. Sci.* **22,** (2021).
733 32. Miller, K. N., Victorelli, S. G., Salmonowicz, H., Dasgupta, N., Liu, T., Passos, J. F. & Adams, P. D.
734 Cytoplasmic DNA: sources, sensing, and role in aging and disease. *Cell* **184,** 5506–5526 (2021).
735 33. Yum, S., Li, M., Fang, Y. & Chen, Z. J. TBK1 recruitment to STING activates both IRF3 and NF-κB
736 that mediate immune defense against tumors and viral infections. *Proceedings of the National*
737 *Academy of Sciences* **118,** e2100225118 (2021).
738 34. Decout, A., Katz, J. D., Venkatraman, S. & Ablasser, A. The cGAS–STING pathway as a
739 therapeutic target in inflammatory diseases. *Nat. Rev. Immunol.* **21,** 548–569 (2021).
740 35. Kreienkamp, R., Graziano, S., Coll-Bonfill, N., Bedia-Diaz, G., Cybulla, E., Vindigni, A., Dorsett, D.,
741 Kubben, N., Batista, L. F. Z. & Gonzalo, S. A Cell-Intrinsic Interferon-like Response Links
742 Replication Stress to Cellular Aging Caused by Progerin. *Cell Rep.* **22,** 2006–2015 (2018).
743 36. Cheedipudi, S. M., Asghar, S. & Marian, A. J. Genetic Ablation of the DNA Damage Response
744 Pathway Attenuates Lamin-Associated Dilated Cardiomyopathy in Mice. *JACC: Basic to*
745 *Translational Science* (2022). doi:10.1016/j.jacbts.2022.06.015
746 37. King, K. R., Aguirre, A. D., Ye, Y.-X., Sun, Y., Roh, J. D., Ng, R. P., Jr, Kohler, R. H., Arlauckas, S.
747 P., Iwamoto, Y., Savol, A., Sadreyev, R. I., Kelly, M., Fitzgibbons, T. P., Fitzgerald, K. A., Mitchison,
748 T., Libby, P., Nahrendorf, M. & Weissleder, R. IRF3 and type I interferons fuel a fatal response to
749 myocardial infarction. *Nat. Med.* **23,** 1481–1487 (2017).
750 38. Cao, D. J., Schiattarella, G. G., Villalobos, E., Jiang, N., May, H. I., Li, T., Chen, Z. J., Gillette, T. G.
751 & Hill, J. A. Cytosolic DNA Sensing Promotes Macrophage Transformation and Governs
752 Myocardial Ischemic Injury. *Circulation* **137,** 2613–2634 (2018).
753 39. Hu, D., Cui, Y.-X., Wu, M.-Y., Li, L., Su, L.-N., Lian, Z. & Chen, H. Cytosolic DNA sensor cGAS
754 plays an essential pathogenetic role in pressure overload-induced heart failure. *Am. J. Physiol.*
755 *Heart Circ. Physiol.* **318,** H1525–H1537 (2020).
756 40. Yan, M., Li, Y., Luo, Q., Zeng, W., Shao, X., Li, L., Wang, Q., Wang, D., Zhang, Y., Diao, H., Rong,
757 X., Bai, Y. & Guo, J. Mitochondrial damage and activation of the cytosolic DNA sensor
758 cGAS-STING pathway lead to cardiac pyroptosis and hypertrophy in diabetic cardiomyopathy
759 mice. *Cell Death Discov* **8,** 258 (2022).
760 41. Kim, Y. & Zheng, Y. Generation and characterization of a conditional deletion allele for Lmna in
761 mice. *Biochem. Biophys. Res. Commun.* **440,** 8–13 (2013).
762 42. Sohal, D. S., Nghiem, M., Crackower, M. A., Witt, S. A., Kimball, T. R., Tymitz, K. M., Penninger, J.
763 M. & Molkentin, J. D. Temporally regulated and tissue-specific gene manipulations in the adult and
764 embryonic heart using a tamoxifen-inducible Cre protein. *Circ. Res.* **89,** 20–25 (2001).
765 43. Hasper, J., Welle, K., Swovick, K., Hryhorenko, J., Ghaemmaghami, S. & Buchwalter, A. Long

766 lifetime and selective accumulation of the A-type lamins accounts for the tissue specificity of
767 Hutchinson-Gilford progeria syndrome. *bioRxiv* 2023.02.04.527139 (2023).
768 doi:10.1101/2023.02.04.527139
769 44. Guey, B., Wischnewski, M., Decout, A., Makasheva, K., Kaynak, M., Sakar, M. S., Fierz, B. &
770 Ablasser, A. BAF restricts cGAS on nuclear DNA to prevent innate immune activation. *Science*
771 **369,** 823–828 (2020).
772 45. Frittoli, E., Palamidessi, A., Iannelli, F., Zanardi, F., Villa, S., Barzaghi, L., Abdo, H., Cancila, V.,
773 Beznoussenko, G. V., Della Chiara, G., Pagani, M., Malinverno, C., Bhattacharya, D., Pisati, F., Yu,
774 W., Galimberti, V., Bonizzi, G., Martini, E., Mironov, A. A., Gioia, U., Ascione, F., Li, Q., Havas, K.,
775 Magni, S., Lavagnino, Z., Pennacchio, F. A., Maiuri, P., Caponi, S., Mattarelli, M., Martino, S.,
776 d'Adda di Fagagna, F., Rossi, C., Lucioni, M., Tancredi, R., Pedrazzoli, P., Vecchione, A., Petrini,
777 C., Ferrari, F., Lanzuolo, C., Bertalot, G., Nader, G., Foiani, M., Piel, M., Cerbino, R., Giavazzi, F.,
778 Tripodo, C. & Scita, G. Tissue fluidification promotes a cGAS-STING cytosolic DNA response in
779 invasive breast cancer. *Nat. Mater.* **22,** 644–655 (2023).
780 46. Srsen, V., Fant, X., Heald, R., Rabouille, C. & Merdes, A. Centrosome proteins form an insoluble
781 perinuclear matrix during muscle cell differentiation. *BMC Cell Biol.* **10,** 28 (2009).
782 47. Patterson, M., Barske, L., Van Handel, B., Rau, C. D., Gan, P., Sharma, A., Parikh, S., Denholtz,
783 M., Huang, Y., Yamaguchi, Y., Shen, H., Allayee, H., Crump, J. G., Force, T. I., Lien, C.-L., Makita,
784 T., Lusis, A. J., Kumar, S. R. & Sucov, H. M. Frequency of mononuclear diploid cardiomyocytes
785 underlies natural variation in heart regeneration. *Nat. Genet.* **49,** 1346–1353 (2017).
786 48. Maciejowski, J., Li, Y., Bosco, N., Campbell, P. J. & de Lange, T. Chromothripsis and Kataegis
787 Induced by Telomere Crisis. *Cell* **163,** 1641–1654 (2015).
788 49. Maciejowski, J., Chatzipli, A., Dananberg, A., Chu, K., Toufektchan, E., Klimczak, L. J., Gordenin,
789 D. A., Campbell, P. J. & de Lange, T. APOBEC3-dependent kataegis and TREX1-driven
790 chromothripsis during telomere crisis. *Nat. Genet.* **52,** 884–890 (2020).
791 50. Mohr, L., Toufektchan, E., von Morgen, P., Chu, K., Kapoor, A. & Maciejowski, J. ER-directed
792 TREX1 limits cGAS activation at micronuclei. *Mol. Cell* **81,** 724–738.e9 (2021).
793 51. Nader, G. P. de F., Agüera-Gonzalez, S., Routet, F., Gratia, M., Maurin, M., Cancila, V., Cadart, C.,
794 Palamidessi, A., Ramos, R. N., San Roman, M., Gentili, M., Yamada, A., Williart, A., Lodillinsky, C.,
795 Lagoutte, E., Villard, C., Viovy, J.-L., Tripodo, C., Galon, J., Scita, G., Manel, N., Chavrier, P. & Piel,
796 M. Compromised nuclear envelope integrity drives TREX1-dependent DNA damage and tumor cell
797 invasion. *Cell* **184,** 5230–5246.e22 (2021).
798 52. Caravia, X. M., Ramirez-Martinez, A., Gan, P., Wang, F., McAnally, J. R., Xu, L., Bassel-Duby, R.,
799 Liu, N. & Olson, E. N. Loss of function of the nuclear envelope protein LEMD2 causes DNA
800 damage-dependent cardiomyopathy. *J. Clin. Invest.* **132,** (2022).

53. Snider, P., Standley, K. N., Wang, J., Azhar, M., Doetschman, T. & Conway, S. J. Origin of cardiac fibroblasts and the role of periostin. *Circ. Res.* **105,** 934–947 (2009).
54. Lavine, K. J., Epelman, S., Uchida, K., Weber, K. J., Nichols, C. G., Schilling, J. D., Ornitz, D. M., Randolph, G. J. & Mann, D. L. Distinct macrophage lineages contribute to disparate patterns of cardiac recovery and remodeling in the neonatal and adult heart. *Proc. Natl. Acad. Sci. U. S. A.* **111,** 16029–16034 (2014).
55. Matsushima, W., Herzog, V. A., Neumann, T., Gapp, K., Zuber, J., Ameres, S. L. & Miska, E. A. Sequencing cell-type-specific transcriptomes with SLAM-ITseq. *Nat. Protoc.* **14,** 2261–2278 (2019).
56. Jin, S., Guerrero-Juarez, C. F., Zhang, L., Chang, I., Ramos, R., Kuan, C.-H., Myung, P., Plikus, M. V. & Nie, Q. Inference and analysis of cell-cell communication using CellChat. *Nat. Commun.* **12,** 1088 (2021).
57. Jin, L., Hill, K. K., Filak, H., Mogan, J., Knowles, H., Zhang, B., Perraud, A.-L., Cambier, J. C. & Lenz, L. L. MPYS is required for IFN response factor 3 activation and type I IFN production in the response of cultured phagocytes to bacterial second messengers cyclic-di-AMP and cyclic-di-GMP. *J. Immunol.* **187,** 2595–2601 (2011).
58. Schoggins, J. W., MacDuff, D. A., Imanaka, N., Gainey, M. D., Shrestha, B., Eitson, J. L., Mar, K. B., Richardson, R. B., Ratushny, A. V., Litvak, V., Dabelic, R., Manicassamy, B., Aitchison, J. D., Aderem, A., Elliott, R. M., García-Sastre, A., Racaniello, V., Snijder, E. J., Yokoyama, W. M., Diamond, M. S., Virgin, H. W. & Rice, C. M. Pan-viral specificity of IFN-induced genes reveals new roles for cGAS in innate immunity. *Nature* **505,** 691–695 (2014).
59. Zhang, H., Ren, L. & Wu, J. C. New Insights Into the Therapy for Lamin-Associated Dilated Cardiomyopathy∗. *JACC: Basic to Translational Science* **7,** 1246–1248 (2022).
60. Long, Z.-J., Wang, J.-D., Xu, J.-Q., Lei, X.-X. & Liu, Q. cGAS/STING cross-talks with cell cycle and potentiates cancer immunotherapy. *Mol. Ther.* **30,** 1006–1017 (2022).
61. Yang, H., Wang, H., Ren, J., Chen, Q. & Chen, Z. J. cGAS is essential for cellular senescence. *Proc. Natl. Acad. Sci. U. S. A.* **114,** E4612–E4620 (2017).
62. Pathare, G. R., Decout, A., Glück, S., Cavadini, S., Makasheva, K., Hovius, R., Kempf, G., Weiss, J., Kozicka, Z., Guey, B., Melenec, P., Fierz, B., Thomä, N. H. & Ablasser, A. Structural mechanism of cGAS inhibition by the nucleosome. *Nature* **587,** 668–672 (2020).
63. Kujirai, T., Zierhut, C., Takizawa, Y., Kim, R., Negishi, L., Uruma, N., Hirai, S., Funabiki, H. & Kurumizaka, H. Structural basis for the inhibition of cGAS by nucleosomes. *Science* **370,** 455–458 (2020).
64. Li, T. & Chen, Z. J. The cGAS-cGAMP-STING pathway connects DNA damage to inflammation, senescence, and cancer. *J. Exp. Med.* **215,** 1287–1299 (2018).
65. Willaume, S., Rass, E., Fontanilla-Ramirez, P., Moussa, A., Wanschoor, P. & Bertrand, P. A Link

836 between Replicative Stress, Lamin Proteins, and Inflammation. *Genes* **12,** (2021).
837 66. Rouhi, L., Auguste, G., Zhou, Q., Lombardi, R., Olcum, M., Pourebrahim, K., Cheedipudi, S. M.,
838 Asghar, S., Hong, K., Robertson, M. J., Coarfa, C., Gurha, P. & Marian, A. J. Deletion of the Lmna
839 gene in fibroblasts causes senescence-associated dilated cardiomyopathy by activating the
840 double-stranded DNA damage response and induction of senescence-associated secretory
841 phenotype. *J Cardiovasc Aging* **2,** (2022).
842 67. Liu, Y., Chen, X., Zhao, Y., Wang, X.-Y., Luo, Y.-W., Chen, L., Wang, W., Zhong, S., Hu, M., Dai, Z.,
843 Jiang, J., Wang, X., Ji, H., Cheng, X.-X., Zheng, A., Zuo, J., Liu, H., Ma, D., Luo, Z., Cao, F., Hu,
844 S., Huang, A.-L. & Tang, K.-F. Small cytosolic double-stranded DNA represses cyclic GMP-AMP
845 synthase activation and induces autophagy. *Cell Rep.* **42,** 112852 (2023).
846 68. Tschöpe, C., Ammirati, E., Bozkurt, B., Caforio, A. L. P., Cooper, L. T., Felix, S. B., Hare, J. M.,
847 Heidecker, B., Heymans, S., Hübner, N., Kelle, S., Klingel, K., Maatz, H., Parwani, A. S., Spillmann,
848 F., Starling, R. C., Tsutsui, H., Seferovic, P. & Van Linthout, S. Myocarditis and inflammatory
849 cardiomyopathy: current evidence and future directions. *Nat. Rev. Cardiol.* **18,** 169–193 (2020).
850 69. Venturini, G., Alvim, J. M., Padilha, K., Toepfer, C. N., Gorham, J. M., Wasson, L. K., Biagi, D.,
851 Schenkman, S., Carvalho, V. M., Salgueiro, J. S., Cardozo, K. H. M., Krieger, J. E., Pereira, A. C.,
852 Seidman, J. G. & Seidman, C. E. Cardiomyocyte infection by Trypanosoma cruzi promotes innate
853 immune response and glycolysis activation. *Front. Cell. Infect. Microbiol.* **13,** 1098457 (2023).
854 70. Lei, Y., VanPortfliet, J. J., Chen, Y.-F., Bryant, J. D., Li, Y., Fails, D., Torres-Odio, S., Ragan, K. B.,
855 Deng, J., Mohan, A., Wang, B., Brahms, O. N., Yates, S. D., Spencer, M., Tong, C. W., Bosenberg,
856 M. W., West, L. C., Shadel, G. S., Shutt, T. E., Upton, J. W., Li, P. & West, A. P. Cooperative
857 sensing of mitochondrial DNA by ZBP1 and cGAS promotes cardiotoxicity. *Cell* **186,**
858 3013–3032.e22 (2023).
859 71. Buxboim, A., Swift, J., Irianto, J., Spinler, K. R., Dingal, P. C. D. P., Athirasala, A., Kao, Y.-R. C.,
860 Cho, S., Harada, T., Shin, J.-W. & Discher, D. E. Matrix elasticity regulates lamin-A,C
861 phosphorylation and turnover with feedback to actomyosin. *Curr. Biol.* **24,** 1909–1917 (2014).
862 72. Swift, J., Ivanovska, I. L., Buxboim, A., Harada, T., Dingal, P. C. D. P., Pinter, J., Pajerowski, J. D.,
863 Spinler, K. R., Shin, J.-W., Tewari, M., Rehfeldt, F., Speicher, D. W. & Discher, D. E. Nuclear
864 lamin-A scales with tissue stiffness and enhances matrix-directed differentiation. *Science* **341,**
865 1240104 (2013).
866 73. Buxboim, A., Irianto, J., Swift, J., Athirasala, A., Shin, J.-W., Rehfeldt, F. & Discher, D. E.
867 Coordinated increase of nuclear tension and lamin-A with matrix stiffness outcompetes lamin-B
868 receptor that favors soft tissue phenotypes. *Mol. Biol. Cell* **28,** 3333–3348 (2017).
869 74. Nomura, S., Satoh, M., Fujita, T., Higo, T., Sumida, T., Ko, T., Yamaguchi, T., Tobita, T., Naito, A. T.,
870 Ito, M., Fujita, K., Harada, M., Toko, H., Kobayashi, Y., Ito, K., Takimoto, E., Akazawa, H., Morita,

H., Aburatani, H. & Komuro, I. Cardiomyocyte gene programs encoding morphological and functional signatures in cardiac hypertrophy and failure. *Nat. Commun.* **9,** 1–17 (2018).

75. Yamada, S., Ko, T., Hatsuse, S., Nomura, S., Zhang, B., Dai, Z., Inoue, S., Kubota, M., Sawami, K., Yamada, T., Sassa, T., Katagiri, M., Fujita, K., Katoh, M., Ito, M., Harada, M., Toko, H., Takeda, N., Morita, H., Aburatani, H. & Komuro, I. Spatiotemporal transcriptome analysis reveals critical roles for mechano-sensing genes at the border zone in remodeling after myocardial infarction. *Nature Cardiovascular Research* **1,** 1072–1083 (2022).
76. Yamada, S., Ko, T., Ito, M., Sassa, T., Nomura, S., Okuma, H., Sato, M., Imasaki, T., Kikkawa, S., Zhang, B., Yamada, T., Seki, Y., Fujita, K., Katoh, M., Kubota, M., Hatsuse, S., Katagiri, M., Hayashi, H., Hamano, M., Takeda, N., Morita, H., Takada, S., Toyoda, M., Uchiyama, M., Ikeuchi, M., Toyooka, K., Umezawa, A., Yamanishi, Y., Nitta, R., Aburatani, H. & Komuro, I. TEAD1 trapping by the Q353R–Lamin A/C causes dilated cardiomyopathy. *Science Advances* **9,** eade7047 (2023).
77. Quina, L. A., Harris, J., Zeng, H. & Turner, E. E. Specific connections of the interpeduncular subnuclei reveal distinct components of the habenulopeduncular pathway. *J. Comp. Neurol.* **525,** 2632–2656 (2017).
78. Gay, L., Miller, M. R., Ventura, P. B., Devasthali, V., Vue, Z., Thompson, H. L., Temple, S., Zong, H., Cleary, M. D., Stankunas, K. & Doe, C. Q. Mouse TU tagging: a chemical/genetic intersectional method for purifying cell type-specific nascent RNA. *Genes Dev.* **27,** 98–115 (2013).
79. Verzi, M. P., McCulley, D. J., De Val, S., Dodou, E. & Black, B. L. The right ventricle, outflow tract, and ventricular septum comprise a restricted expression domain within the secondary/anterior heart field. *Dev. Biol.* **287,** 134–145 (2005).
80. Frankish, A., Diekhans, M., Jungreis, I., Lagarde, J., Loveland, J. E., Mudge, J. M., Sisu, C., Wright, J. C., Armstrong, J., Barnes, I., Berry, A., Bignell, A., Boix, C., Carbonell Sala, S., Cunningham, F., Di Domenico, T., Donaldson, S., Fiddes, I. T., García Girón, C., Gonzalez, J. M., Grego, T., Hardy, M., Hourlier, T., Howe, K. L., Hunt, T., Izuogu, O. G., Johnson, R., Martin, F. J., Martínez, L., Mohanan, S., Muir, P., Navarro, F. C. P., Parker, A., Pei, B., Pozo, F., Riera, F. C., Ruffier, M., Schmitt, B. M., Stapleton, E., Suner, M.-M., Sycheva, I., Uszczynska-Ratajczak, B., Wolf, M. Y., Xu, J., Yang, Y. T., Yates, A., Zerbino, D., Zhang, Y., Choudhary, J. S., Gerstein, M., Guigó, R., Hubbard, T. J. P., Kellis, M., Paten, B., Tress, M. L. & Flicek, P. GENCODE 2021. *Nucleic Acids Res.* **49,** D916–D923 (2021).
81. Love, M. I., Huber, W. & Anders, S. Moderated estimation of fold change and dispersion for RNA-seq data with DESeq2. *Genome Biol.* **15,** 550 (2014).
82. Zhou, Y., Zhou, B., Pache, L., Chang, M., Khodabakhshi, A. H., Tanaseichuk, O., Benner, C. & Chanda, S. K. Metascape provides a biologist-oriented resource for the analysis of systems-level datasets. *Nat. Commun.* **10,** 1523 (2019).

83. Martin, B. K., Qiu, C., Nichols, E., Phung, M., Green-Gladden, R., Srivatsan, S., Blecher-Gonen, R., Beliveau, B. J., Trapnell, C., Cao, J. & Shendure, J. Optimized single-nucleus transcriptional profiling by combinatorial indexing. *Nat. Protoc.* (2022). doi:10.1038/s41596-022-00752-0

84. Amezquita, R. A., Lun, A. T. L., Becht, E., Carey, V. J., Carpp, L. N., Geistlinger, L., Marini, F., Rue-Albrecht, K., Risso, D., Soneson, C., Waldron, L., Pagès, H., Smith, M. L., Huber, W., Morgan, M., Gottardo, R. & Hicks, S. C. Orchestrating single-cell analysis with Bioconductor. *Nat. Methods* **17,** 137–145 (2020).

85. Herzog, V. A., Reichholf, B., Neumann, T., Rescheneder, P., Bhat, P., Burkard, T. R., Wlotzka, W., von Haeseler, A., Zuber, J. & Ameres, S. L. Thiol-linked alkylation of RNA to assess expression dynamics. *Nat. Methods* **14,** 1198–1204 (2017).

FIGURE 1

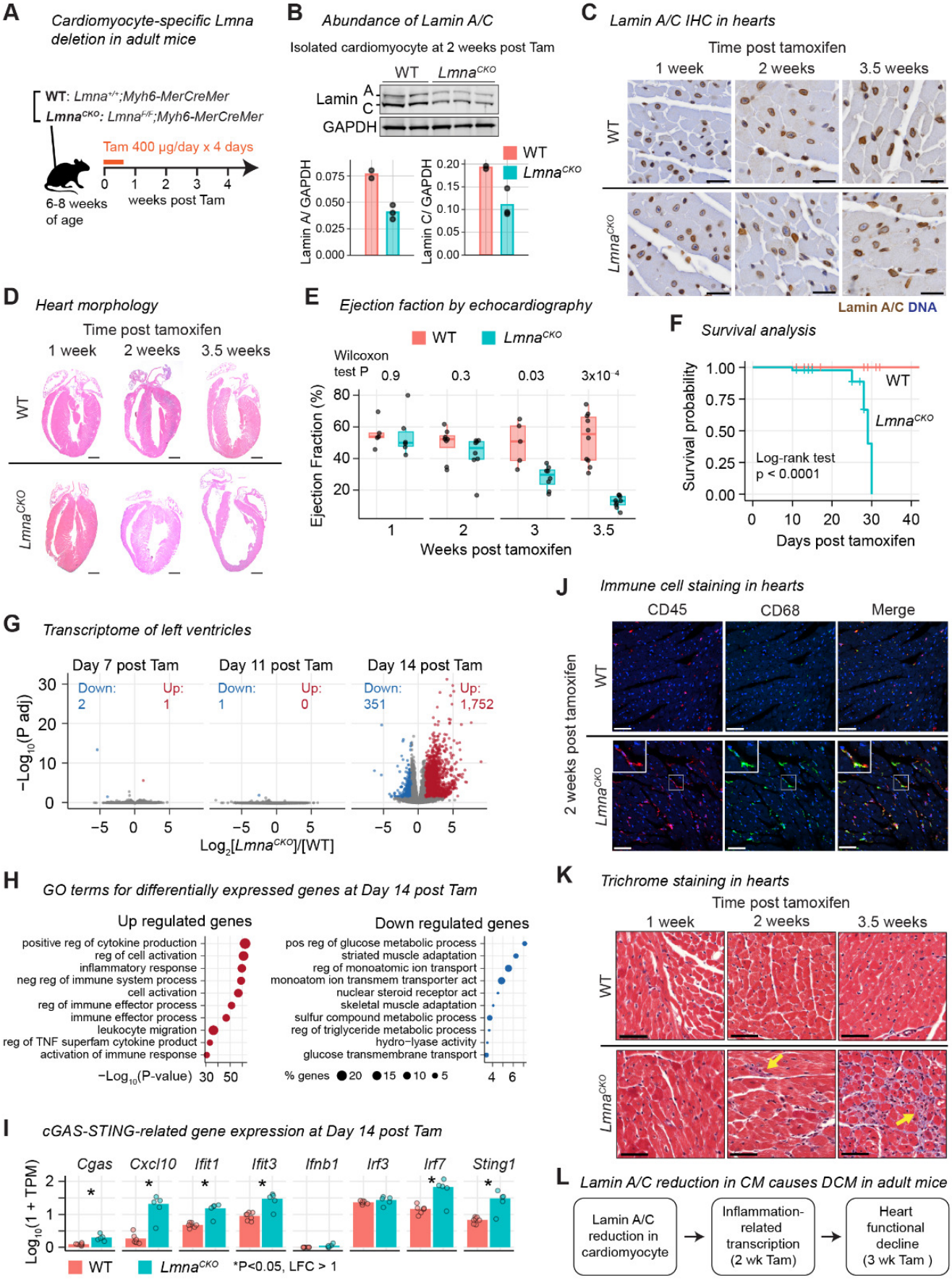
A
Cardiomyocyte-specific Lmna deletion in adult mice
WT: Lmna+/+;Myh6-MerCreMer
LmnaCKO: LmnaF/F;Myh6-MerCreMer
Tam 400 µg/day x 4 days
0 1 2 3 4
weeks post Tam
6-8 weeks of age
B
Abundance of Lamin A/C
Isolated cardiomyocyte at 2 weeks post Tam
WT
LmnaCKO
Lamin A
Lamin C
GAPDH
Lamin A/ GAPDH
Lamin C/ GAPDH
C
Lamin A/C IHC in hearts
Time post tamoxifen
1 week
2 weeks
3.5 weeks
Lamin A/C DNA
D
Heart morphology
E
Ejection faction by echocardiography
Wilcoxon test P
0.9
0.3
0.03
3x10-4
Ejection Fraction (%)
Weeks post tamoxifen
F
Survival analysis
Survival probability
Log-rank test
p < 0.0001
Days post tamoxifen
G
Transcriptome of left ventricles
Day 7 post Tam
Day 11 post Tam
Day 14 post Tam
Down: 2
Up: 1
Down: 1
Up: 0
Down: 351
Up: 1,752
−Log10(P adj)
Log2[LmnaCKO]/[WT]
H
GO terms for differentially expressed genes at Day 14 post Tam
Up regulated genes
positive reg of cytokine production
reg of cell activation
inflammatory response
neg reg of immune system process
cell activation
reg of immune effector process
immune effector process
leukocyte migration
reg of TNF superfam cytokine product
activation of immune response
−Log10(P-value)
Down regulated genes
pos reg of glucose metabolic process
striated muscle adaptation
reg of monoatomic ion transport
monoatom ion transmem transporter act
nuclear steroid receptor act
skeletal muscle adaptation
sulfur compound metabolic process
reg of triglyceride metabolic process
hydro−lyase activity
glucose transmembrane transport
% genes
I
cGAS-STING-related gene expression at Day 14 post Tam
Cgas
Cxcl10
Ifit1
Ifit3
Ifnb1
Irf3
Irf7
Sting1
Log10(1 + TPM)
*P<0.05, LFC > 1
J
Immune cell staining in hearts
CD45
CD68
Merge
2 weeks post tamoxifen
K
Trichrome staining in hearts
L
Lamin A/C reduction in CM causes DCM in adult mice
Lamin A/C reduction in cardiomyocyte
Inflammation-related transcription (2 wk Tam)
Heart functional decline (3 wk Tam)

Figure 1. Lamin A/C reduction in cardiomyocytes causes dilated cardiomyopathy in adult mice

A) Tamoxifen treatment (Tam) deletes *Lmna* in cardiomyocytes in mice at 6-8 weeks of age.
B) Top: Lamin A/C immunoblot for cardiomyocytes isolated from two wild-type and three $Lmna^{CKO}$ mice. Bottom: Quantification of immunoblot signals.
C) Lamin A/C immunohistochemistry (brown) with hematoxylin counterstaining (blue) in mouse heart tissues (60×). Scale bar: 20 μm.
D) Hematoxylin/eosin staining of whole hearts. Scale bar: 1 mm.
E) Left ventricular ejection fraction (EF) measured by echocardiography. Dot, EF of individual mice. Boxplot, interquartile range.
F) Kaplan-Meier survival plot. WT, n=48. $Lmna^{CKO}$, n=42.
G) Volcano plot contrasting gene expression in $Lmna^{CKO}$ versus WT left ventricles, determined by RNA-seq. Upregulated (up) or downregulated (down) genes at $P < 0.05$ with Log_2 fold change > 1.
H) The top 10 Gene Ontology terms overrepresented among differentially expressed genes.
I) Normalized gene expressed levels (TPM) from RNA-seq data for the cGAS-STING pathway-related genes. Dot, individual mouse TPM. Bar, mean of biological replicates (WT, n=7. $Lmna^{CKO}$, n=5).
J) Immunofluorescence of heart tissue sections for CD45 (pan-leukocyte, red) and CD68 (macrophage, green). Scale bar: 20 μm. Quantification, **Fig. S1**.
K) Masson's trichrome staining of heart sections. Arrow, collagen deposition. Scale bar: 20 μm.
L) Timeline of events.

SUPPLEMENTARY FIGURE S1

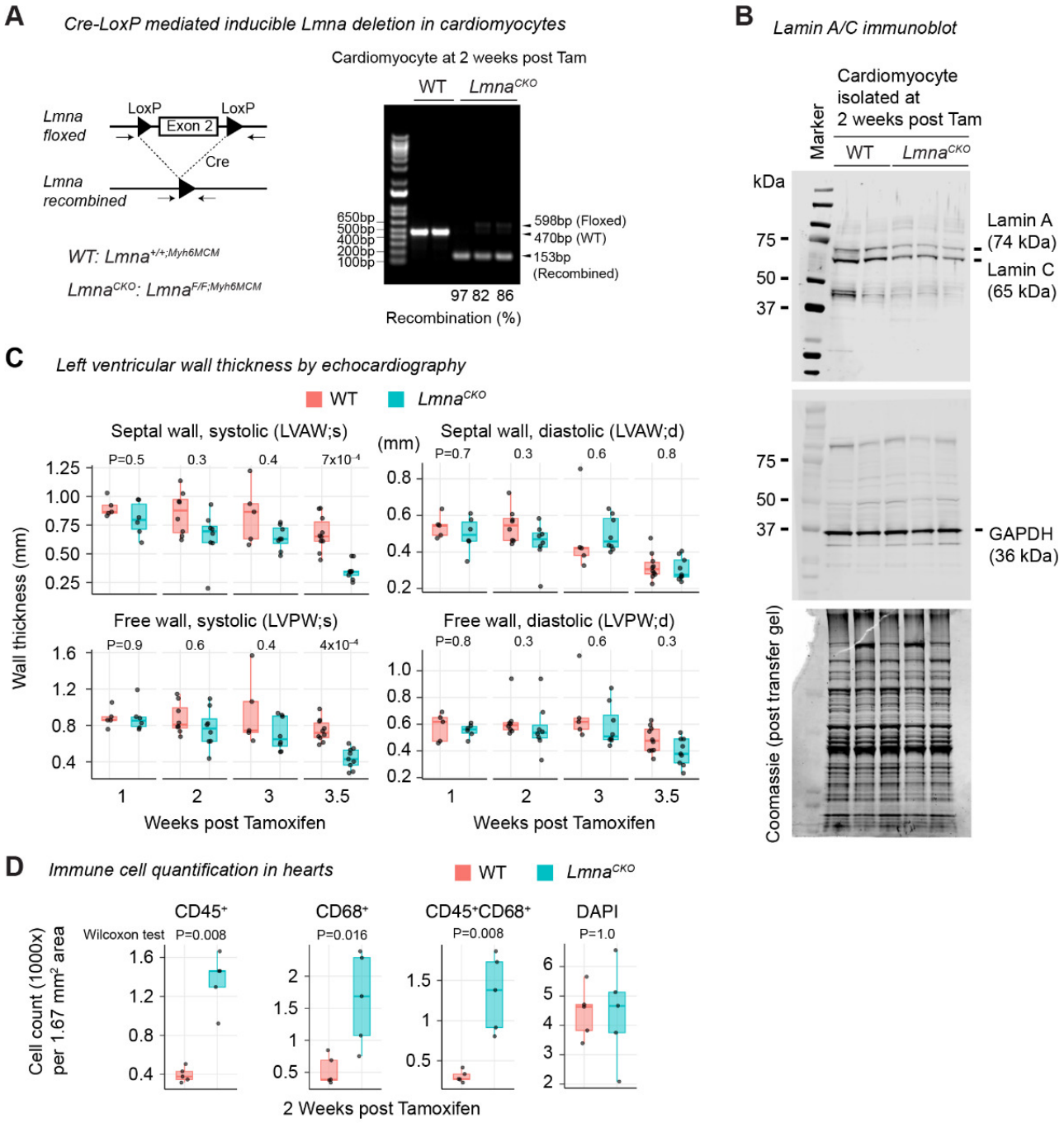

Supplementary Figure S1. Characterization of cardiomyocyte-specific deletion of *Lmna* in adult mice

A) Left: *Lmna* LoxP allele and the expected recombined allele by Cre expression. Arrow, PCR primer location. Right: PCR detection of the recombined (deleted) allele in *Lmna*^{CKO} cardiomyocytes. Recombination (%), 153-bp band (Recombined) over 598-bp band (Floxed) intensities.
B) Whole immunoblot for Lamin A/C and GAPDH, and Coomassie staining of original gel, in isolated cardiomyocytes. Part is shown in **Fig. 1B**.
C) M-mode echocardiography of left ventricular (LV) geometry. P, Wilcoxon test.
D) Quantification of CD45 and CD68-positive cells in heart sections. Representative image in Fig. 1J.

FIGURE 2

A *Lamin A/C immunohistochemistry of heart*

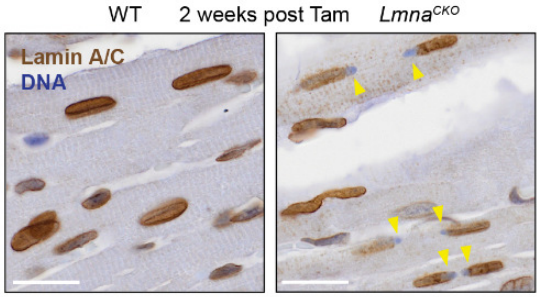

B *Electronmicroscopy of heart*

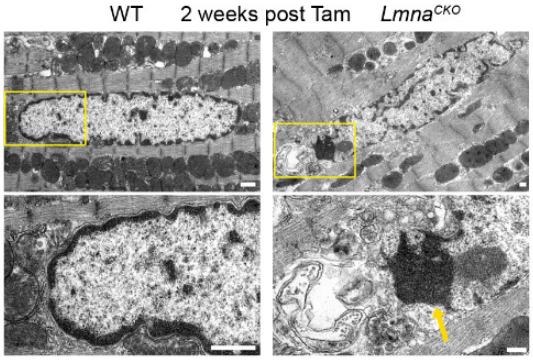

C *Lamin A/C & PCM IF in isolated cardiomyocyte*

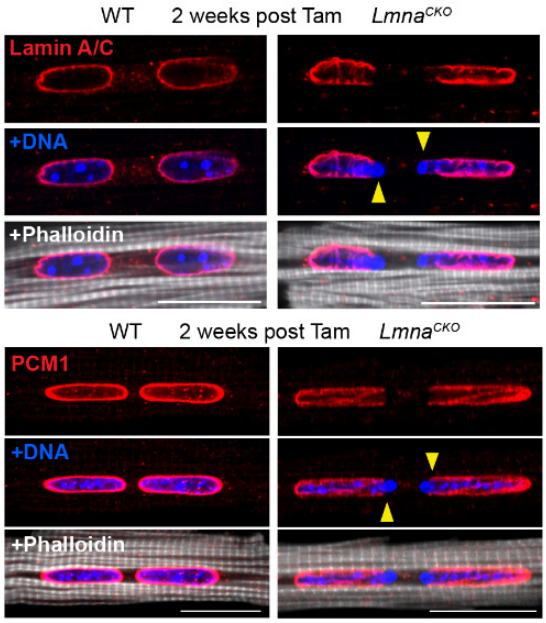

D *NE rupture frequency*

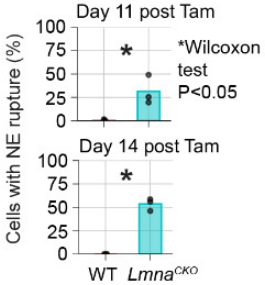

E *Number of ruptured nuclei per cell*

		No. ruptured nuclei per cell		
		0	1	≥2
% Cells (count)	Day 11 post Tam, WT	99% (163)	1% (1)	0% (0)
	Day 11 post Tam, *Lmna*^{CKO}	69% (121)	14% (25)	17% (30)
	Day 14 post Tam, WT	100% (163)	0% (0)	0% (0)
	Day 14 post Tam, *Lmna*^{CKO}	46% (78)	25% (42)	29% (49)

F *Localization of NLS-tdTomato in isolated cardiomyocyte*

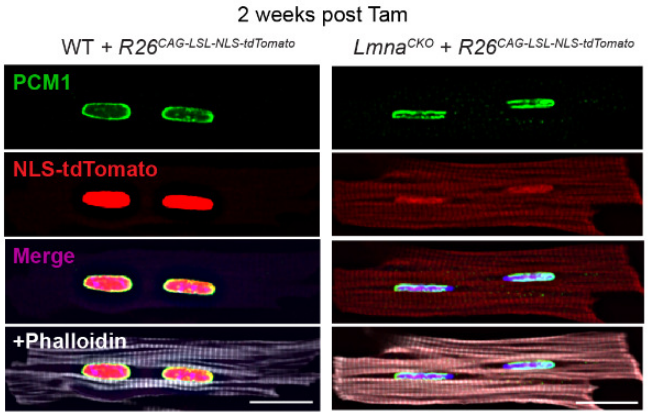

G *Quantification of tdTomato signal*

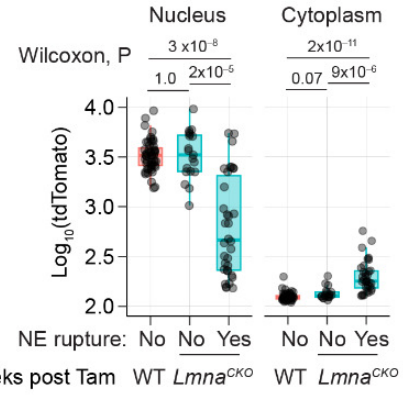

H *γ-H2AX IF in heart*

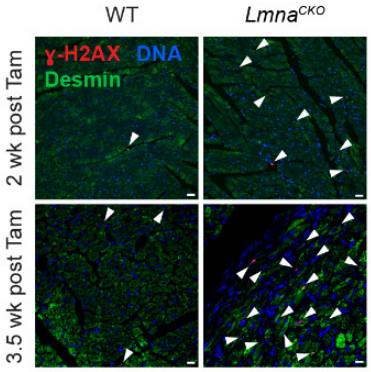

I *TUNEL assay in heart*

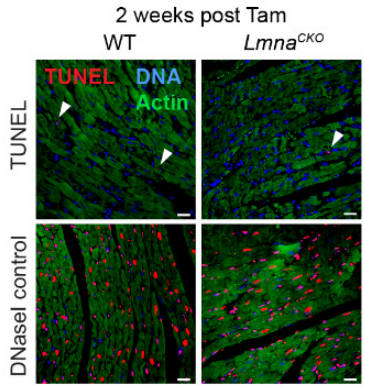

J *TUNEL quantification*

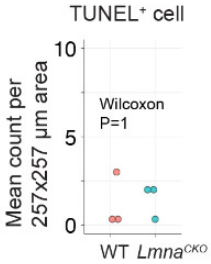

K *NE rupture precedes transcriptional alteration*

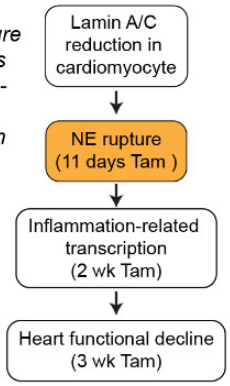

Fig. 2. Lamin A/C reduction causes localized nuclear envelope rupture in cardiomyocytes

A) Lamin A/C immunohistochemistry in heart tissue. Arrow, nuclear DNA protruded from nuclei. Scale bar: 20 μm.
B) Top: Transmission electron micrograph of heart sections focusing on cardiomyocytes. Bottom: Enlarged images of the area indicated by the yellow box in the upper panel. Arrow, protruded chromatin. Scale bar: 20 μm.
C) Immunofluorescence for Lamin A/C (top) and PCM1 (bottom) in isolated cardiomyocytes. Phalloidin stains F-actin. Arrowhead, nuclear envelope rupture. Scale bar: 20 μm.
D) Percentage of isolated multinucleated cardiomyocytes with nuclear envelope ruptures, defined by DNA protrusion from PCM1-lost nuclear tips. Mean percentage (bar) of three biological replicates (dots).
E) Multinucleated cardiomyocyte count by the number of ruptured nuclei per cell.
F) Immunofluorescence for PCM-1 with detection of native NLS-tdTomato. Scale bar: 20 μm.
G) Quantification of NLS-tdTomato intensity in the nucleus and the cytoplasm. WT, n=51. *Lmna*^{CKO}, n=53 (ruptured 34, unruptured 19).
H) Immunofluorescence for γH2AX and desmin in heart tissue sections. Desmin stains cardiomyocytes. Arrowhead, γH2AX-stained nuclei. Scale bar: 20 μm.
I) TUNEL assay for cell death detection in heart tissues. DNaseI treatment of tissues serves as a positive control (bottom). Arrowhead, TUNEL-positive cells. Scale bar: 20 μm.
J) Quantification of TUNEL-positive cells. Dot, mean TUNEL-positive cell count in 2–3 images per mouse. n=3 mice per genotype.
K) Timeline of events.

SUPPLEMENTARY FIGURE S2

A *Additional images for EM in hearts*

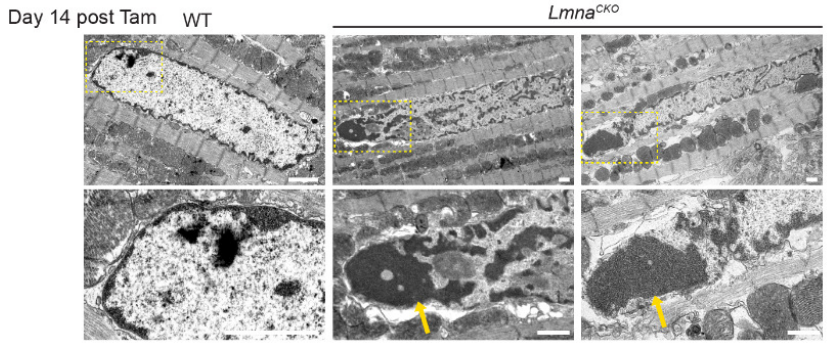

B *Additional images for Lamin A/C IF in CMs at Day 14 post Tam*

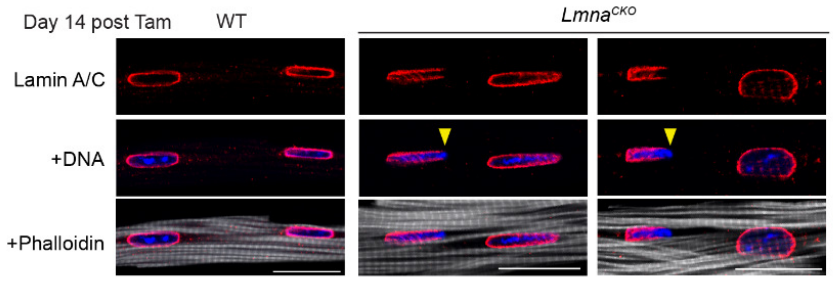

C *PCM1 IF in CMs at Day 11 post Tam*

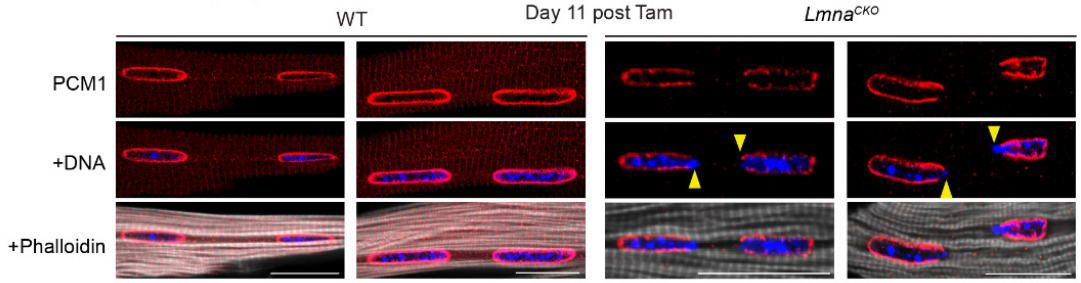

D *PCM1 IF in CMs at Day 14 post Tam*

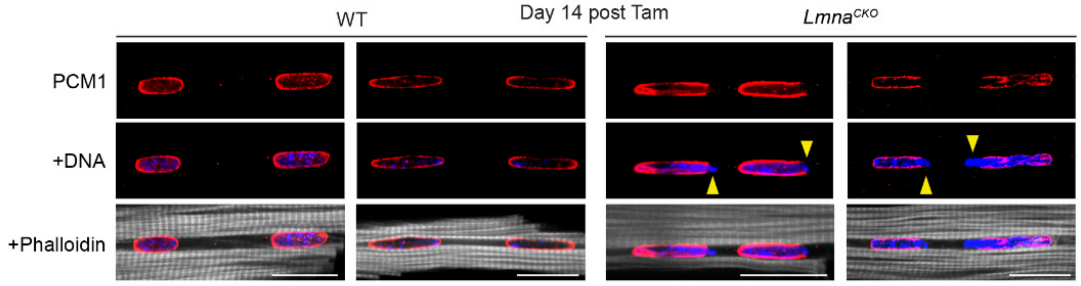

E *Additional images for NLS-tdTomato signals in Lmna^{CKO} CMs*

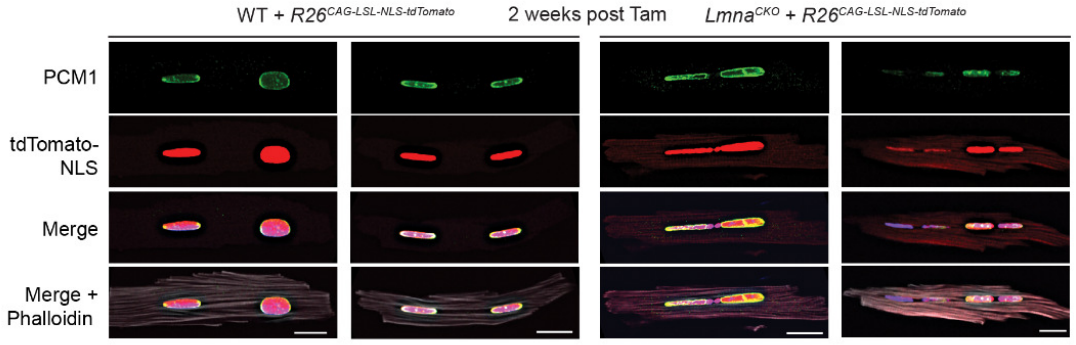

Supplementary Figure S2. Characterization of nuclear envelope ruptures in *Lmna*^{CKO} cardiomyocytes

A) Top: Additional transmission electron micrographs of heart sections focusing on cardiomyocytes, related to **Fig. 2B**. Bottom: Enlarged images of the area indicated by yellow box in the upper panels. Arrow, protruded chromatin. Scale bar: 20 µm.
B) Additional immunofluorescence images for Lamin A/C in isolated cardiomyocytes at 2 weeks post tamoxifen, related to **Fig. 2C**. Phalloidin stains F-actin. Arrowhead, nuclear envelope rupture. Scale bar: 20 µm.
C) Same as (B), but for PCM1 at Day 11 post tamoxifen.
D) Same as (C), but for Day 14 post tamoxifen.
E) Additional immunofluorescence images for PCM-1 with detection of native NLS-tdTomato. Scale bar: 20 µm.

SUPPLEMENTARY FIGURE S3

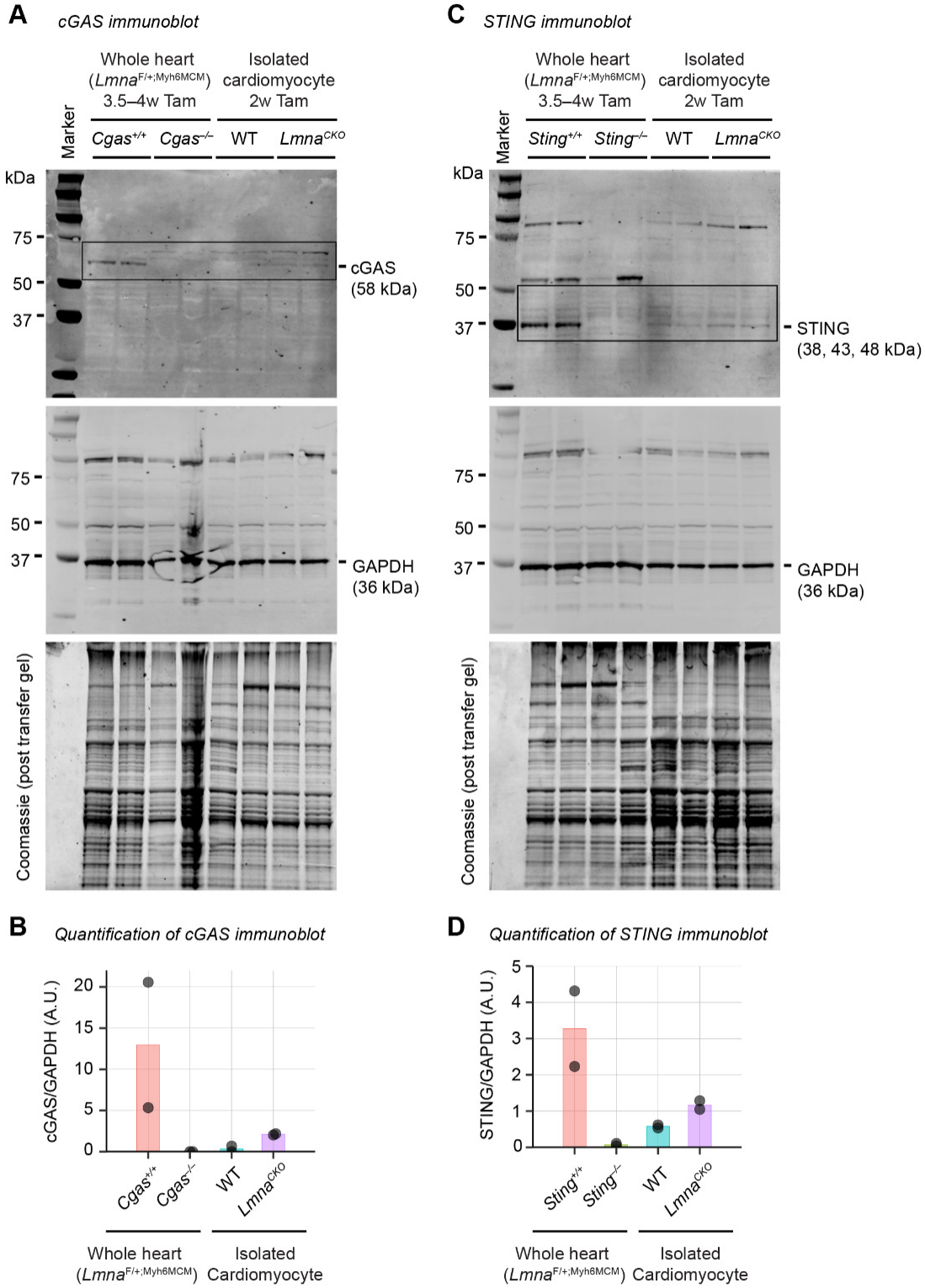

Supplementary Figure S3. Protein abundance of cGAS and STING in hearts and cardiomyocytes.

A) Immunoblot for cGAS and GAPDH, and Coomassie staining of original gel, in hearts and isolated cardiomyocytes.
B) Quantification of cGAS immunoblot. The intensity of cGAS is normalized by GAPDH.
C) Same as (A), but for STING.
D) Same as (B), but for STING immunoblot.

FIGURE 3

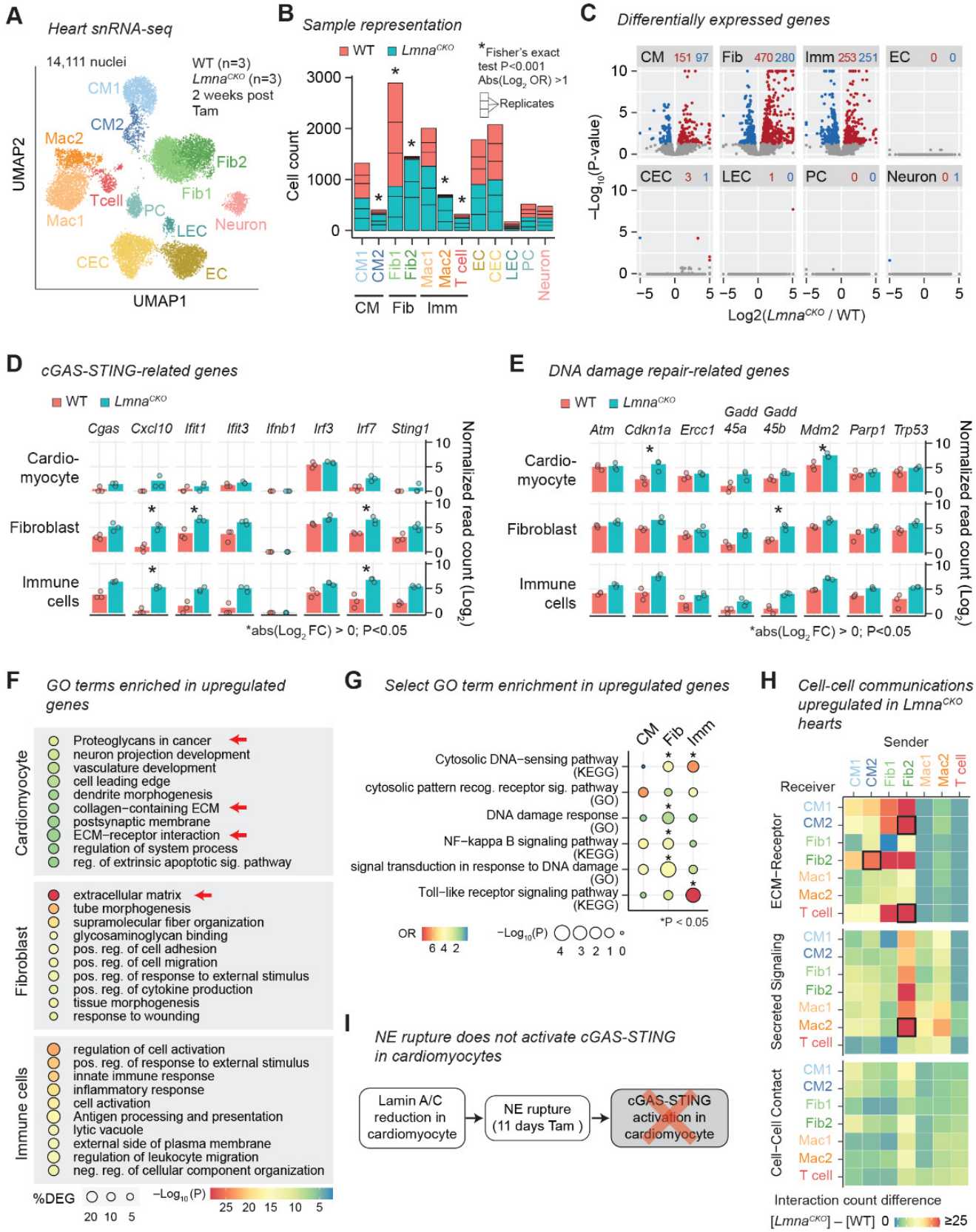
A
Heart snRNA-seq
14,111 nuclei
WT (n=3)
Lmna^CKO (n=3)
2 weeks post Tam
CM1
CM2
Mac2
Fib2
Fib1
Tcell
PC
Mac1
LEC
Neuron
CEC
EC
UMAP2
UMAP1
B
Sample representation
WT
Lmna^CKO
*Fisher's exact test P<0.001 Abs(Log2 OR) >1
Replicates
Cell count
CM
Fib
Imm
C
Differentially expressed genes
CM 151 97
Fib 470 280
Imm 253 251
EC 0 0
CEC 3 1
LEC 1 0
PC 0 0
Neuron 0 1
−Log10(P-value)
Log2(Lmna^CKO / WT)
D
cGAS-STING-related genes
Cgas
Cxcl10
Ifit1
Ifit3
Ifnb1
Irf3
Irf7
Sting1
Cardio-myocyte
Fibroblast
Immune cells
Normalized read count (Log2)
*abs(Log2 FC) > 0; P<0.05
E
DNA damage repair-related genes
Atm
Cdkn1a
Ercc1
Gadd 45a
Gadd 45b
Mdm2
Parp1
Trp53
F
GO terms enriched in upregulated genes
Cardiomyocyte
Proteoglycans in cancer
neuron projection development
vasculature development
cell leading edge
dendrite morphogenesis
collagen−containing ECM
postsynaptic membrane
ECM−receptor interaction
regulation of system process
reg. of extrinsic apoptotic sig. pathway
Fibroblast
extracellular matrix
tube morphogenesis
supramolecular fiber organization
glycosaminoglycan binding
pos. reg. of cell adhesion
pos. reg. of cell migration
pos. reg. of response to external stimulus
pos. reg. of cytokine production
tissue morphogenesis
response to wounding
Immune cells
regulation of cell activation
pos. reg. of response to external stimulus
innate immune response
inflammatory response
cell activation
Antigen processing and presentation
lytic vacuole
external side of plasma membrane
regulation of leukocyte migration
neg. reg. of cellular component organization
%DEG
−Log10(P)
G
Select GO term enrichment in upregulated genes
Cytosolic DNA−sensing pathway (KEGG)
cytosolic pattern recog. receptor sig. pathway (GO)
DNA damage response (GO)
NF−kappa B signaling pathway (KEGG)
signal transduction in response to DNA damage (GO)
Toll−like receptor signaling pathway (KEGG)
*P < 0.05
OR
−Log10(P)
H
Cell-cell communications upregulated in Lmna^CKO hearts
Sender
Receiver
ECM−Receptor
Secreted Signaling
Cell−Cell Contact
Interaction count difference
[Lmna^CKO] – [WT]
≥25
I
NE rupture does not activate cGAS-STING in cardiomyocytes
Lamin A/C reduction in cardiomyocyte
NE rupture (11 days Tam)
cGAS-STING activation in cardiomyocyte

Figure 3. Absence of the cGas-STING pathway activation within *Lmna*^{CKO} cardiomyocytes

A) snRNA-seq UMAP plot for 14,111 nuclei, originating from WT (n=3) and *Lmna*^{CKO} (n=3) hearts at 2 weeks post tamoxifen, colored by cell-type annotation. CM, cardiomyocyte. Fib, fibroblast. Mac, macrophage. EC, endothelial cell. CEC, coronary EC. LEC, lymphatic EC. PC, pericyte.
B) Nuclei count for the 6 samples (WT x3, *Lmna*^{CKO} x3) within each cell type cluster of snRNA-seq in **A**.
C) Volcano plot contrasting gene expression in cells of *Lmna*^{CKO} hearts versus cells of WT hearts within each cell type, determined by snRNA-seq in **A**. Red, upregulated genes. Blue, downregulated genes at $P < 0.05$ with Log_2 fold change > 1. CM, CM1 + CM2. Fib, Fib1 + Fib2. Imm (immune cells), Mac1 + Mac2 + T cells.
D) Expression (mean of single-nucleus normalized read count within cell type) of cGAS-STING pathway-related genes. Data are from snRNA-seq in **A**. Dot, mean within individual mice. Bar, mean across three mice.
E) Same as (D), but for DNA damage response-related genes.
F) Top 10 most enriched GO terms associated with upregulated genes within indicated cell type, defined in **C**. Arrow, ECM-related pathways.
G) Enrichment for select GO terms relevant to cytosolic DNA sensing among upregulated genes, defined in **C**.
H) Predicted difference in signaling interactions between *Lmna*^{CKO} hearts and WT hearts. Each cell in the matrix represents the differential signaling score for a given sender–receiver pair. Data are from snRNA-seq in **A**. Square, strong interactions noted in the text.
I) Timeline of events.

SUPPLEMENTARY FIGURE S4

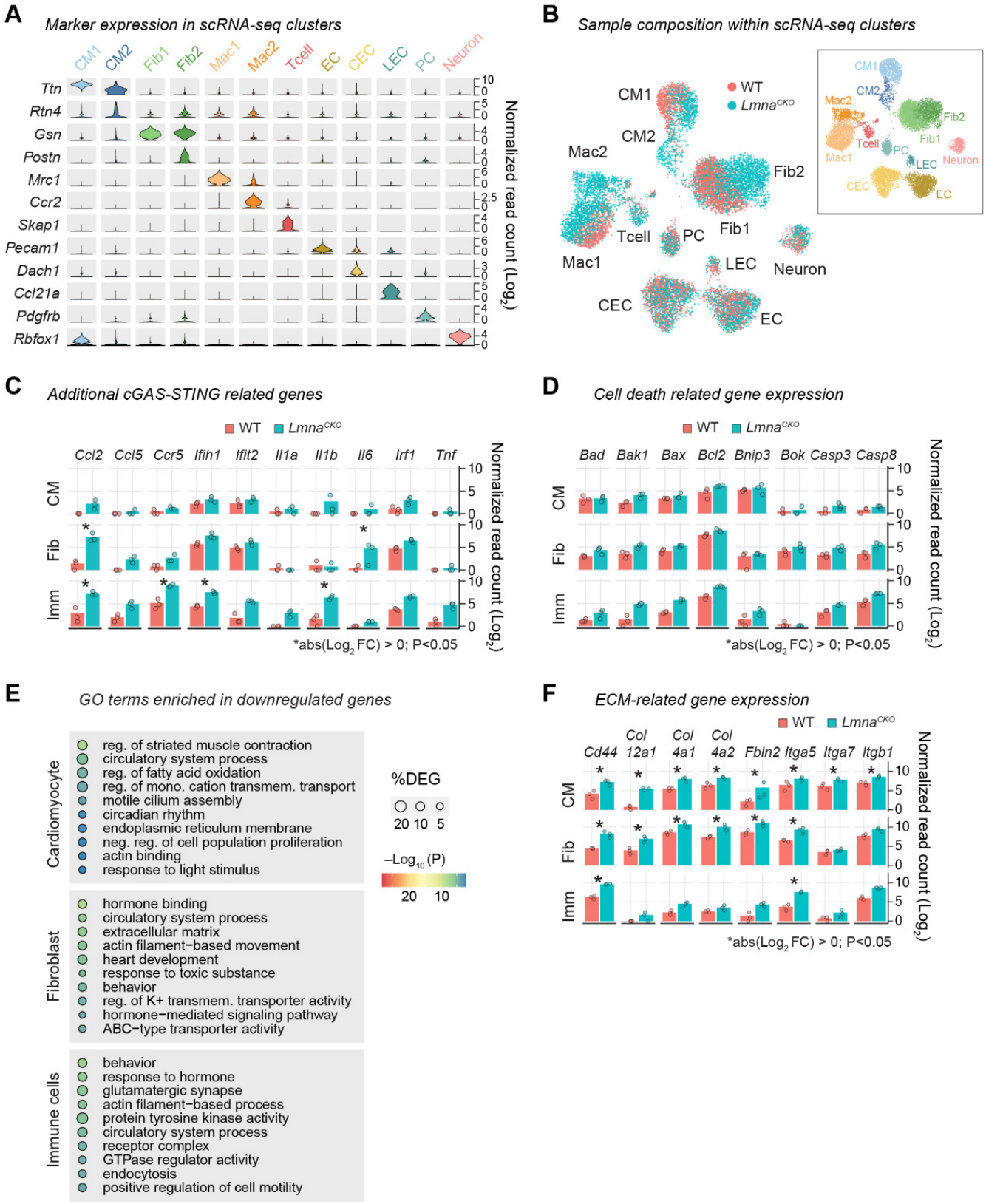

Supplementary Figure S4. Single-nucleus RNA-seq analysis in *Lmna*^{CKO} heart

A) Expression (sum of single-nucleus normalized read count across 3 mice within cell type) of marker genes used to classify single nuclei to the cell types indicated on the Y axis.
B) snRNA-seq UMAP plot for 14,111 nuclei, colored by sample genotype. Inset, UMAP colored by cell type for reference.
C) Expression (mean of single-nucleus normalized read count within cell type) of additional cGAS-STING pathway-related genes, related to **Fig. 3D**. Dot, mean within individual mice. Bar, mean across three mice.
D) Same as (C), but for cell death-related genes.
E) Top 10 most enriched GO terms associated with downregulated genes within indicated cell type.
F) Same as (C), but for ECM-related genes.

SUPPLEMENTARY FIGURE S5

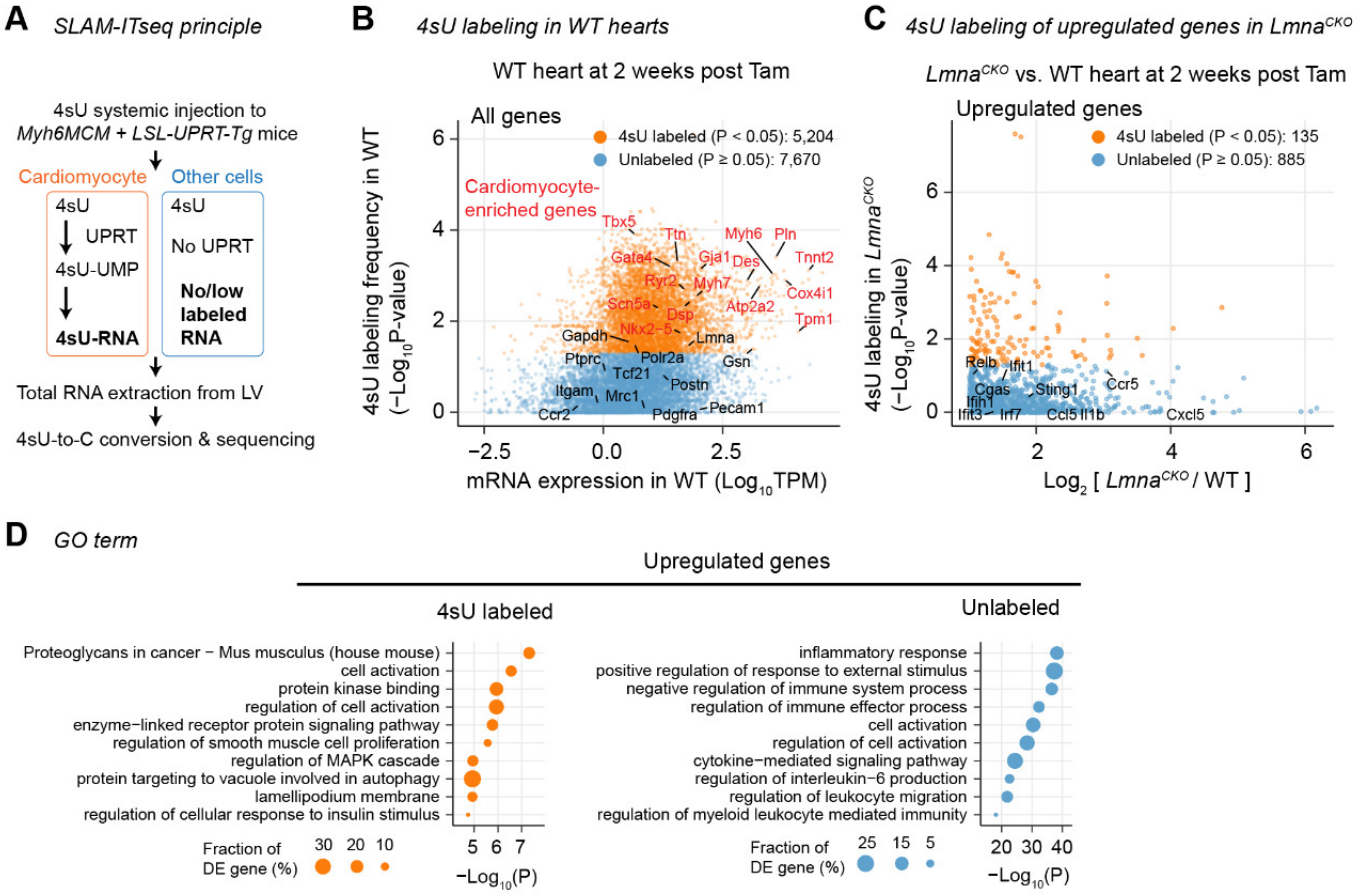

Supplementary Figure S5. SLAM-IT-seq analysis in *Lmna*^{CKO} heart

A) Principle of SLAM-IT-seq. Transcripts in cardiomyocytes are labeled by 4-thiouracil (4sU).
B) SLAM-IT-seq data for all genes in WT hearts at 2 weeks post tamoxifen, with the expression level on the X axis and the 4sU labeling frequency on the Y axis. Known cardiomyocyte-enriched genes (red) and other select genes (black) are indicated.
C) SLAM-IT-seq data for upregulated genes at 2 weeks post tamoxifen, with the expression difference on the X axis and the 4sU labeling frequency in *Lmna*^{CKO} hearts on the Y axis. All cytokine genes among the upregulated genes are indicated.
D) GO terms for 4sU labeled or unlabeled upregulated genes.

FIGURE 4

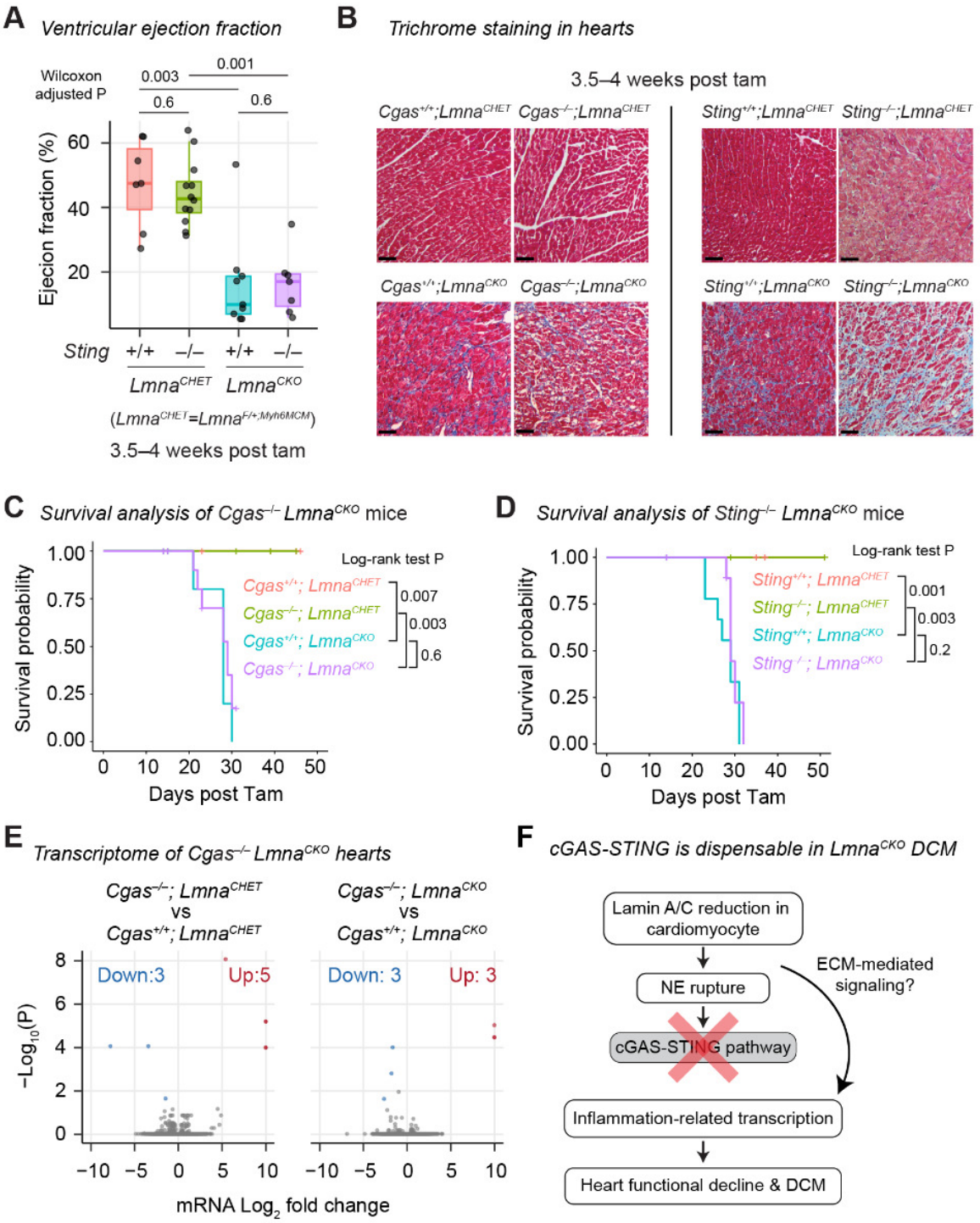

Fig. 4. *Cgas* or *Sting* deletion does not rescue dilated cardiomyopathy in *Lmna*^{CKO} mice

A) Left ventricular ejection fraction (EF) measured by echocardiography. *Lmna*^{CHET}, *Lmna*$^{F/+;Myh6MCM}$ mice. Dot, EF of individual mice. Boxplot, interquartile range. *Sting*$^{+/+}$; *Lmna*^{CHET}, n=7. *Sting*$^{-/-}$; *Lmna*^{CHET}, n=12. *Sting*$^{+/+}$; *Lmna*^{CKO}, n=9. *Sting*$^{-/-}$; *Lmna*^{CKO}, n=7.
B) Trichrome-stained heart sections. Scale bar: 20 µm.
C) Kaplan-Meier survival plot. *Cgas*$^{+/+}$; *Lmna*^{CHET}, n=13. *Cgas*$^{-/-}$; *Lmna*^{CHET}, n=12. *Cgas*$^{+/+}$; *Lmna*^{CKO}, n=13. *Cgas*$^{-/-}$; *Lmna*^{CKO}, n=14.
D) Kaplan-Meier survival plot. *Sting*$^{+/+}$; *Lmna*^{CHET}, n=5. *Sting*$^{-/-}$; *Lmna*^{CHET}, n=8. *Sting*$^{+/+}$; *Lmna*^{CKO}, n=11. *Sting*$^{-/-}$; *Lmna*^{CKO}, n=11.

E) Volcano plot contrasting gene expression in *Cgas*$^{-/-}$; *Lmna*^{CHET} (n=4) versus *Cgas*$^{+/+}$; *Lmna*^{CHET} (n=6) (left) and in *Cgas*$^{-/-}$; *Lmna*^{CKO} (n=4) versus *Cgas*$^{+/+}$; *Lmna*^{CKO} (n=6) (right). Upregulated (up) or downregulated (down) genes at $P < 0.05$ with Log_2 fold change > 1.
F) Summary: The cGAS-STING pathway does not mediate the development of dilated cardiomyopathy in *Lmna*^{CKO} mice.